Theoretical and Experimental Investigations on Dynamic Penetration Test Apparatus

Shigeru KITAGO

(Received July 30, 1960)

Contents

Abstract

Dynamic penetration test was investigated theoretically and experimentally, from a standpoint of the driving equipment, ie., rammer, driving rod and driving point etc., and not from the foundation soil penetrated by the driving point. Fundamental equations were introduced, which give strains created by the impact at the supported end, as an application of a longitudinal vibration problem of

a straight bar, in which one end is supported elastically, and the other is struck by a rammer longitudinally. Many factors affecting penetration resistance may be explained; for example, effects of rod length, rammer weight and its drop height on exerted strains at the end of the rod. Laboratory experiments were undertaken to show the correctness of the fundamental equations, the results of which have been in close agreement with the theory.

Part. I Theoretical Investigation

1. Fundamental Equations

The dynamic penetration test can be regarded as an impact problem of a bar, where one end is supported elastically and the other is struck longitudinally by a rammer, when the foundation soils are assumed to be elastic. The solution of a similar kind of problem with one end fixed, has been given by Boussinesq and St. Venant, the details of which are fully explained in the references 1), 2) and 3). By an addition of a following boundary condition at $x=0$, in Fig. 1,

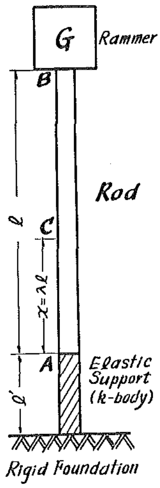

Fig. 1. Longitudinal impact of rod.

$$EA\frac{\partial u}{\partial x}=pu$$

to the case of the fixed end, instead of $u=0$, at $x=0$, the two functions of longitudinal stress wave, $F(at+x)$ and $f(at-x)$ can be acquired in the same manner as in the special case of the fixed end, in which;

$E=$ Young's modulus of elasticity of a penetration rod

$A=$ sectional area of the rod

$u=$ elastic vertical displacement in the rod at a distance x from the supported end as in Fig. 1

$p=$ force necessary for producing unit depression at $x=0$ in the elastic body which supports the end of the rod in place of the ground soil. This material will be referred to as a k-body hereinafter.

$F(at+x)=$ stress function in the elastic rod, travelling downwards from B to A in Fig. 1

$f(at-x)=$ stress function in the elastic rod, travelling upwards from A to B in the same figure

$t=$ time measured from the instant of impact by the rammer

$a=$ propagation velocity of stress wave in elastic materials

$=\sqrt{\dfrac{Eg}{\gamma}}$, where g is the acceleration of gravity and γ is the density of rod material, while compression is assumed to be negative.

When the two functions of the stress wave are obtained, the strain at any point and at any time may be calculated as follows;

$$\frac{\partial u}{\partial x}=-f'(at-x)+F'(at+x) \tag{1}$$

The stress and the total force created by the impact at the point and at the time are accordingly calculated as $E\dfrac{\partial u}{\partial x}$ and $EA\dfrac{\partial u}{\partial x}$.

Original forms of the fundamental functions f and F are different for each vibration period as seen in the references 1), 2) and 3), and also the equations for the strain due to longitudinal impact are different for each period of vibration. The periods of vibration at $x=\lambda l$ are divided as follows, substituting τl for x into equation (1);

1-a the earlier part of the first period $(1-\lambda)<\tau<(1+\lambda)$, which corresponds to the time interval from the arrival of the first downward stress wave at point C in Fig. 1, until the reflected longitudinal wave reaches the point for the first time,

1-b the later part of the first period, $(1+\lambda)<\tau<(3-\lambda)$, which corresponds to the time interval from the arrival of the first reflected wave at point C, until the second downward wave of longitudinal vibration reaches the point C in question,

and in the same manner for the second and the third period,

2-a the earlier part of the second period, $(3-\lambda)<\tau<(3+\lambda)$;

2-b the later part of the second period, $(3+\lambda)<\tau<(5-\lambda)$;

3-a the earlier part of the third period, $(5-\lambda)<\tau<(5+\lambda)$;

3-b the later part of the third period, $(5+\lambda)<\tau<(7-\lambda)$;

and so on. The vibration periods of the stress wave at the points $x=0$ or $x=l$ can be obtained by placing $\lambda=0$ or 1 into the above periods, although $3<\tau<3$ in the earlier period 2-a for $\lambda=0$ means $\tau=3$ and it gives the displacement u or the strain $\dfrac{\partial u}{\partial x}$ at the instant of $\tau=3$.

The strains exerted by the impact at any point C in Fig. 1 for each period are as follows; the process of determining the original functions of f and F will be omitted here, because the details are fully explained in the references of 1), 2) and 3);

1-a $(1-\lambda)<\tau<(1+\lambda)$, the earlier part of the first period

$$\frac{\partial u}{\partial x}=-\frac{V}{a}\cdot e^{-\alpha}\cdot e^{-(\tau-1)/m} \tag{2}$$

1–b $(1+\lambda)<\tau<(3-\lambda)$, the later part of the first period

$$\frac{\partial u}{\partial x}=\frac{V}{a}\left[(Me^{\alpha}-e^{-\alpha})e^{-(\tau-1)/m}-Me^{\beta}\cdot e^{-kl(\tau-1)}\right] \tag{3}$$

2–a $(3-\lambda)<\tau<(3+\lambda)$, the earlier part of the second period

$$\frac{\partial u}{\partial x}=\frac{V}{a}\Big[(Me^{\alpha}-e^{-\alpha})e^{-(\tau-1)/m}-M(M+2\alpha)e^{-\alpha}\cdot e^{-(\tau-3)/m}$$
$$-\frac{2M}{m}e^{-\alpha}\cdot e^{-(\tau-3)/m}\cdot(\tau-3)+\left\{M^{2}e^{(2-\lambda)kl}-Me^{\beta}\right\}e^{-kl(\tau-1)}\Big] \tag{4}$$

2–b $(3+\lambda)<\tau<(5-\lambda)$, the later part of the second period

$$\frac{\partial u}{\partial x}=\frac{V}{a}\Big[(Me^{\alpha}-e^{-\alpha})e^{-(\tau-1)/m}-M^{2}\left\{\left(1+\frac{2\alpha}{M}\right)e^{-\alpha}+\left(2\alpha-\frac{1+6q+q^{2}}{1-q^{2}}\right)e^{\alpha}\right\}e^{-(\tau-3)/m}$$
$$+\frac{2M}{m}(Me^{\alpha}-e^{-\alpha})e^{-(\tau-3)/m}\cdot(\tau-3)-M\cdot e^{\beta}\cdot e^{-kl(\tau-1)}$$
$$+M^{2}\left\{e^{-\beta}-\left(\frac{1+6q+q^{2}}{1-q^{2}}+2\beta\right)e^{\beta}\right\}e^{-kl(\tau-3)}+2klM^{2}e^{\beta}e^{-kl(\tau-3)}\cdot(\tau-3)\Big] \tag{5}$$

3–a $(5-\lambda)<\tau<(5+\lambda)$, the earlier part of the third period

$$\frac{\partial u}{\partial x}=\frac{V}{a}\Big[(Me^{\alpha}-e^{-\alpha})e^{-(\tau-1)/m}-M^{2}\left\{\left(2\alpha-\frac{1+6q+q^{2}}{1-q^{2}}\right)e^{\alpha}+\left(1+\frac{2\alpha}{M}\right)e^{-\alpha}\right\}e^{-(\tau-3)/m}$$
$$-M^{2}e^{-\alpha}\left\{\frac{1+10q+q^{2}}{(1-q)^{2}}+\frac{12q+4q^{2}}{1-q^{2}}\alpha+2\alpha^{2}\right\}e^{-(\tau-5)/m}$$
$$+M^{2}\cdot\frac{2}{m}\left(e^{\alpha}-\frac{1}{M}e^{-\alpha}\right)e^{-(\tau-3)/m}\cdot(\tau-3)-\frac{4M^{2}}{m}e^{-\alpha}\left\{\frac{3q+q^{2}}{1-q^{2}}+\alpha\right\}e^{-(\tau-5)/m}\cdot(\tau-5)$$
$$-\frac{2M^{2}}{m^{2}}\cdot e^{-\alpha}e^{-(\tau-5)/m}\cdot(\tau-5)^{2}-Me^{\beta}\cdot e^{-kl(\tau-1)}$$
$$+M^{2}\left\{e^{-\beta}-\left(\frac{1+6q+q^{2}}{1-q^{2}}+2\beta\right)e^{\beta}\right\}e^{-kl(\tau-3)}$$
$$+M^{2}e^{-\beta}\left\{\frac{1+10q+q^{2}}{(1-q)^{2}}-2\beta M\right\}e^{-kl(\tau-5)}+2klM^{2}\cdot e^{\beta}\cdot e^{-kl(\tau-3)}\cdot(\tau-3) \tag{6}$$

3–b $(5+\lambda)<\tau<(7-\lambda)$, the later part of the third period

$$
\begin{aligned}
\frac{\partial u}{\partial x} = \frac{V}{a}\Bigg[& (Me^{\alpha}-e^{-\alpha})e^{-(\tau-1)/m}-M^2\Bigg\{\left(2\alpha-\frac{1+6q+q^2}{1-q^2}\right)e^{\alpha}+\left(1+\frac{2\alpha}{M}\right)e^{-\alpha}\Bigg\}e^{-(\tau-3)/m} \\
& -M^2\Bigg\{\left(\frac{1+10q+q^2}{(1-q)^2}+\frac{12q+4q^2}{1-q^2}\alpha+2\alpha^2\right)e^{-\alpha}-\Bigg(\frac{1+20q+54q^2+20q^3+q^4}{(1+q)(1-q)^3} \\
& -\frac{20q+4q^2}{(1-q)^2}\alpha+2\alpha^2M\Bigg)e^{\alpha}\Bigg\}e^{-(\tau-5)/m}-\frac{2}{m}M^2\left(\frac{1}{M}e^{-\alpha}-e^{\alpha}\right)e^{-(\tau-3)/m}\cdot(\tau-3) \\
& -\frac{4}{m}M^2\Bigg\{\left(\frac{3q+q^2}{1-q^2}+\alpha\right)e^{-\alpha}-\left(\frac{5q+q^2}{(1-q)^2}-\alpha M\right)e^{\alpha}\Bigg\}e^{-(\tau-5)/m}\cdot(\tau-5) \\
& -\frac{2M^2}{m^2}\Big\{e^{-\alpha}-Me^{\alpha}\Big\}e^{-(\tau-5)/m}\cdot(\tau-5)^2-Me^{\beta}\cdot e^{-kl(\tau-1)} \\
& +M^2\Bigg\{e^{-\beta}-\left(\frac{1+6q+q^2}{1-q^2}+2\beta\right)e^{\beta}\Bigg\}e^{-kl(\tau-3)}+M^2\Bigg\{\left(\frac{1+10q+q^2}{(1-q)^2}-2\beta M\right)e^{-\beta} \\
& -\left(\frac{1+20q+54q^2+20q^3+q^4}{(1+q)(1-q)^3}+\frac{4+20q}{(1-q)^2}\cdot\beta+2\beta^2M\right)e^{\beta}\Bigg\}e^{-kl(\tau-5)} \\
& +2klM^2e^{\beta}\cdot e^{-kl(\tau-3)}\cdot(\tau-3)+M^2\Bigg\{\left(kl\frac{4+20q}{(1-q)^2}+4kl\beta M\right)e^{\beta}-2klMe^{-\beta}\Bigg\} \\
& \times e^{-kl(\tau-5)}\cdot(\tau-5)-2k^2l^2M^3\cdot e^{\beta}\cdot e^{-kl(\tau-5)}\cdot(\tau-5)^2\Bigg]
\end{aligned}
\tag{7}
$$

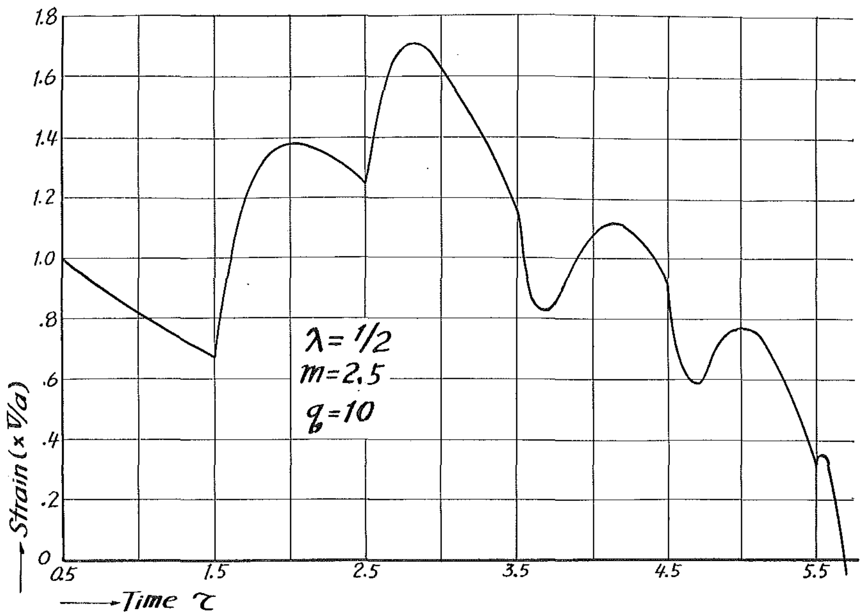

Fig. 2. Strain-time curve for centre of rod.

where

$\alpha = \lambda/m$ (dimensionless)
$\beta = \lambda kl$ (dimensionless)
$k = p/EA$ (cm^{-1})
$m = G/\gamma Al$ (dimensionless)
$q = klm$ (dimensionless)
G = weight of rammer (kg)
$M = (1+q)/(1-q)$ (dimensionless)
V = velocity of rammer at the instant of impact (cm/sec)

Fig. 2 is an example of strain-time curve for $\lambda=0.5$, $m=2.5$ and $q=10$.

In the various problems of dynamic penetration test or pile driving, it is necessary to know how much stress or total force is exerted by the impact at the point of the end of the rod and not at the other part of the rod. If strains are determined, stresses and total forces are easily calculated as mentioned before. Then the strains at the supported end can automatically be obtained by placing $\alpha=\beta=0$ in equations (2) to (7), as follows;

1. $1<\tau<3$, the first period

$$\frac{\partial u}{\partial x}=\frac{V}{a}M^2\left[\frac{2q(1-q)}{(1+q)^2}e^{-(\tau-1)/m}-\frac{1}{M}e^{-kl(\tau-1)}\right] \tag{8}$$

2. $3<\tau<5$, the second period

$$\frac{\partial u}{\partial x}=\frac{V}{a}M^2\left[\frac{2q(1-q)}{(1+q)^2}e^{-(\tau-1)/m}+\frac{6q+2q^2}{1-q^2}e^{-(\tau-3)/m}+\frac{4q}{m(1+q)}e^{-(\tau-3)/m}\cdot(\tau-3)\right.$$
$$\left.-\frac{1}{M}e^{-kl(\tau-1)}-\frac{6q+2q^2}{1-q^2}e^{-kl(\tau-3)}+2kle^{-kl(\tau-3)}\cdot(\tau-3)\right] \tag{9}$$

3. $5<\tau<7$, the third period

$$\frac{\partial u}{\partial x}=\frac{V}{a}M^2\left[\frac{2q(1-q)}{(1+q)^2}e^{-(\tau-1)/m}+\frac{6q+2q^2}{1-q^2}e^{-(\tau-3)/m}+\frac{10q+54q^2+30q^3+2q^4}{(1+q)(1-q)^3}e^{-(\tau-5)/m}\right.$$
$$+\frac{4q}{m(1+q)}e^{-(\tau-3)/m}\cdot(\tau-3)+\frac{8q+32q^2+8q^3}{m(1+q)(1-q)^2}e^{-(\tau-5)/m}\cdot(\tau-5)$$
$$+\frac{4q}{m^2(1-q)}e^{-(\tau-5)/m}\cdot(\tau-5)^2-\frac{1}{M}e^{-kl(\tau-1)}-\frac{6q+2q^2}{1-q^2}e^{-kl(\tau-3)}$$
$$-\frac{10q+54q^2+30q^3+2q^4}{(1+q)(1-q)^3}e^{-kl(\tau-5)}+2kle^{-kl(\tau-3)}\cdot(\tau-3)$$
$$\left.+2kl\frac{1+10q+q^2}{(1-q)^2}e^{-kl(\tau-5)}\cdot(\tau-5)-2k^2l^2Me^{-kl(\tau-5)}\cdot(\tau-5)^2\right] \tag{10}$$

4. $7<\tau<9$, the fourth period

$$\frac{\partial u}{\partial x}=\frac{V}{a}M^2\Big[\frac{2q(1-q)}{(1+q)^2}e^{-(\tau-1)/m}+\frac{6q+2q^2}{1-q^2}e^{-(\tau-3)/m}+\frac{10q+54q^2+30q^3+2q^4}{(1+q)(1-q)^3}e^{-(\tau-5)/m}$$

$$+\frac{14q+202q+588q^3+404q^4+70q^5+2q^6}{(1+q)(1-q)^5}e^{-(\tau-7)/m}$$

$$+\frac{4q}{m(1+q)}e^{-(\tau-3)/m}\cdot(\tau-3)+\frac{8q+32q^2+8q^3}{m(1+q)(1-q)^2}e^{-(\tau-5)/m}\cdot(\tau-5)$$

$$+\frac{12q+144q^2+328q^3+144q^4+12q^5}{m(1+q)(1-q)^4}e^{-(\tau-7)/m}\cdot(\tau-7)+\frac{4q}{m^2(1-q)}e^{-(\tau-5)/m}\cdot(\tau-5)^2$$

$$+\frac{4q+48q^2+12q^3}{m^2(1-q)^3}e^{-(\tau-7)/m}\cdot(\tau-7)^2+\frac{8q(1+q)}{3m^3(1-q)^2}e^{-(\tau-7)/m}\cdot(\tau-7)^3$$

$$-\frac{1}{M}e^{-kl(\tau-1)}-\frac{6q+2q^2}{1-q^2}e^{-kl(\tau-3)}-\frac{10q+54q^2+30q^3+2q^4}{(1+q)(1-q)^3}e^{-kl(\tau-5)}$$

$$-\frac{14q+202q^2+588q^3+404q^4+70q^5+2q^6}{(1+q)(1-q)^5}e^{-kl(\tau-7)}+2kle^{-kl(\tau-3)}\cdot(\tau-3)$$

$$+2kl\frac{1+10q+q^2}{(1-q)^2}e^{-kl(\tau-5)}\cdot(\tau-5)+2kl\frac{1+28q+102q+28q^3+q^4}{(1-q)^4}e^{-kl(\tau-7)}\cdot(\tau-7)$$

$$-2k^2l^2Me^{-kl(\tau-5)}\cdot(\tau-5)^2-2k^2l^2\frac{2+16q+14q^2}{(1-q)^3}e^{-kl(\tau-7)}\cdot(\tau-7)^2$$

$$+4k^3l^3\frac{(1+q)^2}{3(1-q)^2}e^{-kl(\tau-7)}\cdot(\tau-7)^3\Big] \qquad (11)$$

By the equations (8), (9), (10) and (11), the strain at any given moment, hence the stresses and the total forces at the elastically supported end can be calculated, when weight of rammer, drop height, rod length, mechanical proporites of rod and condition of k-body are given.

2. Comparison with the fixed end problem

Boussinesq and St. Venant have given the following results of the strains at $x=0$ in the problem of longitudinal impact of a bar with a fixed end:

1. $1<\tau<3$, the first period

$$\left(\frac{\partial u}{\partial x}\right)_{\substack{x=0\\k=\infty}}=-2\frac{V}{a}e^{-(\tau-1)/m} \qquad (12)$$

2. $3<\tau<5$, the second period

$$\left(\frac{\partial u}{\partial x}\right)_{\substack{x=0\\k=\infty}} = -2\frac{V}{a}\left\{e^{-(\tau-1)/m}+e^{-(\tau-3)/m}-\frac{2}{m}e^{-(\tau-3)/m}\cdot(\tau-3)\right\} \tag{13}$$

3. $5<\tau<7$, the third period

$$\left(\frac{\partial u}{\partial x}\right)_{\substack{x=0\\k=\infty}} = -2\frac{V}{a}\left\{e^{-(\tau-1)/m}+e^{-(\tau-3)/m}+e^{-(\tau-5)/m}-\frac{2}{m}e^{-(\tau-3)/m}\cdot(\tau-3)\right.$$
$$\left.-\frac{4}{m}e^{-(\tau-5)/m}\cdot(\tau-5)+\frac{2}{m^2}e^{-(\tau-5)/m}\cdot(\tau-5)^2\right\} \tag{14}$$

4. $7<\tau<9$, the fourth period

$$\left(\frac{\partial u}{\partial x}\right)_{\substack{x=0\\k=\infty}} = -2\frac{V}{a}\left\{e^{-(\tau-1)/m}+e^{-(\tau-3)/m}+e^{-(\tau-5)/m}+e^{-(\tau-7)/m}-\frac{2}{m}e^{-(\tau-3)/m}\cdot(\tau-3)\right.$$
$$-\frac{4}{m}e^{-(\tau-5)/m}\cdot(\tau-5)-\frac{6}{m}e^{-(\tau-7)/m}\cdot(\tau-7)+\frac{2}{m^2}e^{-(\tau-5)/m}\cdot(\tau-5)^2$$
$$\left.+\frac{6}{m^2}e^{-(\tau-7)/m}\cdot(\tau-7)^2-\frac{4}{3m^2}e^{-(\tau-7)/m}\cdot(\tau-7)^3\right\} \tag{15}$$

Substituting $k=\infty$, which means at the same time $q=\infty$, into the equations (8), (9), (10) and (11), the above four equations are easily obtained and this shows that the equations (8), (9), (10) and (11) are applicable to general cases, while the equations (12), (13), (14) and (15) are applicable to special cases.

3. Strain calculation

Fig. 3 shows some strain-τ curves for 3 kinds of m and q, which demonstrate the functions of m and q in each case. In the horizontal direction, the curves show the function of q which is proportional to the elastic property of the k-body. q is klm as defined before, but it can be transformed as follows;

$$q=klm=kl\frac{G}{\gamma Al}=k\frac{G}{\gamma A}$$

When the weight of the rammer and the dimensions of penetration rod are known, q is proportional to k, and thus q may be considered to be proportional to the elastic property of the k-body. On the other hand, in the vertical direction of Fig. 3, the curves demonstrate the function of m, which is reversely proportional to rod length when $G/\gamma A$ is constant.

From Fig. 3, it may be said that;

1. The duration of impact becomes longer, as the value of m increases, and shorter, as the value of q increases. The impact ceases at the instant when

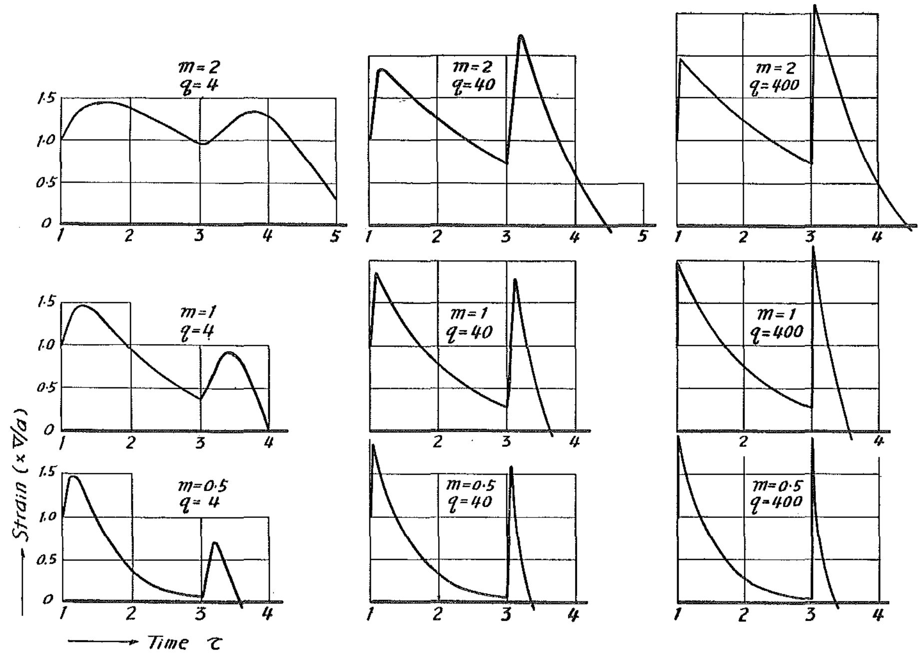

Fig. 3. Strain-time curves for several combinations of m and q.

the strain changes its sign from compression to tension.

2. The impact strain jumps soon after $\tau=1$ or 3, but not exactly at $\tau=1$ or 3, whereas in the case of the fixed end it jumps exactly at $\tau=1$ or 3 to the extent of $\frac{2V}{a}$, as clearly seen in the equations (12), (13) and so on. This shows that sudden changes of stress occur at the time of the arrival of each stress wave having a downward direction in the case of the fixed end, and after it, in the case of the elastic end.

3. The travelling distance of the strain wave before changing its direction becomes shorter as the value of m decreases and that of q increases.

4. The peak values of the strain become larger, as the values of m and q increase.

5. While m is small, the maximum value of strain occurs in the first period, and its absolute value is the same for a given value of q, irrespective of the values of k, l and m, where q is klm as stated before. The time of its occurence, however, becomes later as m increases. These are very interesting and are explained later.

6. As the value of m increases, the maximum strain takes place in the second

or third period. The value of τ which gives the maximum strain for various combinations of m and q is shown in Fig. 4.

The characteristics of strain curves in the case of Boussinesq and St. Venant's fixed end theory are minutely described in the reference 3).

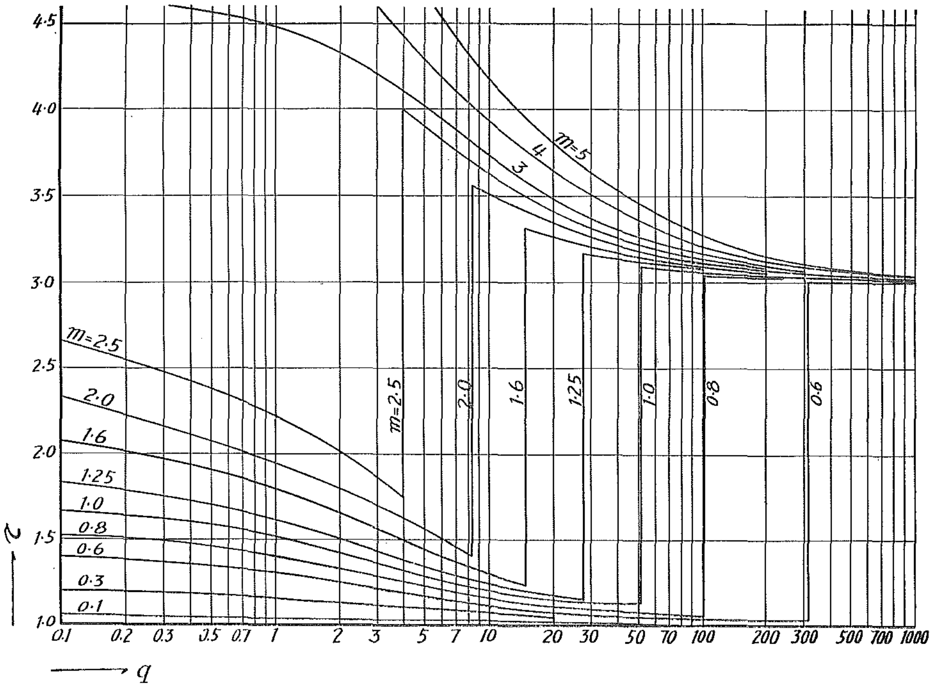

Fig. 4. Values of τ, which give the maximum strain.

What is usually required in a practical dynamic penetration test is the maximum strain created by the impact at the elastic end. These maximum strains can be obtained in the following two manners.

Strain in the first period

It is easy to find a peak value within this period, and if this value is larger than that for the second or the third period, it can be regarded as the maximum strain for one assumed condition of dynamic penetration. A peak value for the first period of vibration can be calculated by the equation (16), which can be obtained by differentiating the equation (8) with τ and rendering the result of the differentiation zero.

$$\left(\frac{\partial u}{\partial x}\right)_{\substack{\max \\ 1<\tau<3}} = \frac{V}{a}\left\{\frac{2q}{1+q}e^{-\frac{1}{1-q}\log\frac{2}{1+q}} - Me^{-M\log\frac{2}{1+q}}\right\} \tag{16}$$

The value of τ which gives this strain is also acquired as follows :

$$\tau=1+\frac{m}{1+q}\log\frac{2}{1+q} \tag{17}$$

The strain by the equation (16) will be the maximum for the whole period of impact, if it is larger than the peak strains occuring in the successive periods of vibration. The equation (16) shows that the strain in the first period is a function of q only, when V and a are assumed to be constant. Then it may be concluded that the maximum strain at the elastic end, when it occurs in the first period, is independent of rod length l, since q is $kG/\gamma A$ as shown before, and independent of l.

It is also clear from the equation (16) that the maximum strain, when it appears in this period, is the same for a certain value of q, irrespective of the values of k, l and m, as stated before, insofar as the values of m and q are less than a certain magnitude.

The equation (17) shows that the time at which the strain jumps is not at $\tau=1$, but a little after $\tau=1$. Numerical calculations for the second and the third period also show that the strain jumps after $\tau=3$ or 5. If $q=\infty$ is substituted into the equation (17), τ is calculated as a unity and it corresponds to a special case of the fixed end.

Strain in the second or the third period

It is not easy to obtain a peak value for the second or the third period, and the trial method of calculation is only applicable to these higher periods, while the peak value for the first period can readily be obtained by the equation (16).

Fig. 5 shows the maximum strain curves for various combinations of m and q and the bottom curve of them corresponds to that of the first period, which is independent of rod length under a certain condition of m and q. For example, when m is less than 2, the maximum strain is independent of m, insofar as q is less than 8.4. The curves which branch out from the bottom curve belongs to the second period, and the greater part of those for $m=3$, 4 and 5, also belong to the same period, whereas a portion of these curves contains the vibration of the third period, in which q has a comparatively smaller value. Numerical calculation has shown that the maximum strain had not appeared in the fourth period insofar as the values of m and q in Fig. 5 are concerned.

The characteristics of these curves will be explained in Part II with the discussions of the experimental test results, while experimentation was not undertaken on wave velocity a, and this term is shortly explained.

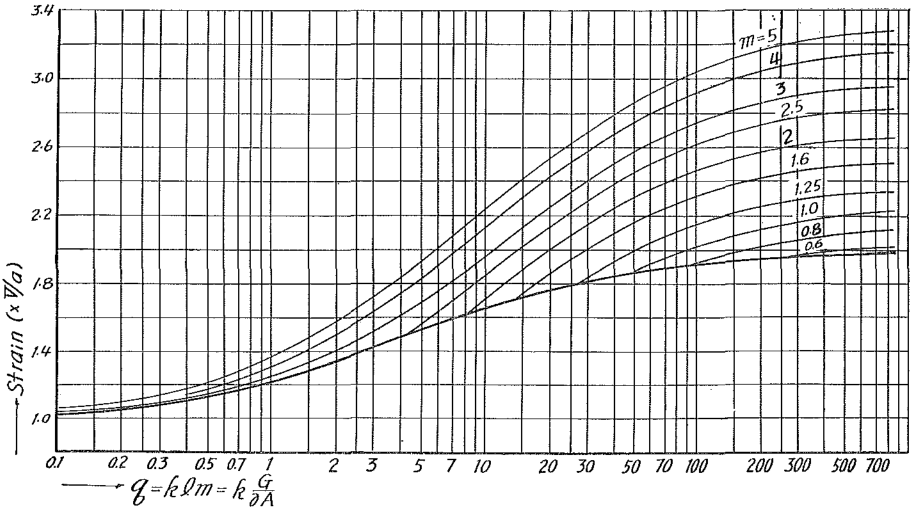

Fig. 5. Strain-m, q curves.

Effects on the strain at the end of the rod due to wave velocity a are those affected by the mechanical properties of the rod material, namely Young's modulus and the density of the rod itself. Then it can easily be understood that this term has almost nothing to do with the dynamic penetration test, because the values of E and γ do not vary insofar as only one type of test equipment is used during the investigation. But in pile driving problems, several kinds of material are used, and so this term must have a significant meaning. It may be predicted from Fig. 5 that steel pile can transmit impact forces to the end of the pile far better than concrete or wooden piles under the same condition of impact.

Part. II Experimental Investigation

Laboratory experiments were undertaken to show the correctness of the fundamental equations concerning the basis of dynamic penetration tests or pile driving, from which the present author expects to draw some conclusions on various factors affecting the test results of dynamic penetration or pile driving.

As it was previously mentioned, the foundation soil is assumed to be elastic, and so in this experiment some elastic materials which were called k-bodies were used as an elastic support of the rod in place of soil which would be penetrated by the sounding rod or driven by piles.

1. Test equipment and methods

(1) Rods and rod support

Three kinds of rods were prepared as shown in Table 1, from which the general purposes of the investigations on types and properties of driving rod can be seen.

TABLE 1. Test Rods

Series	Designation	Length and joints	Weight	Diametre	Section	Material
P	l	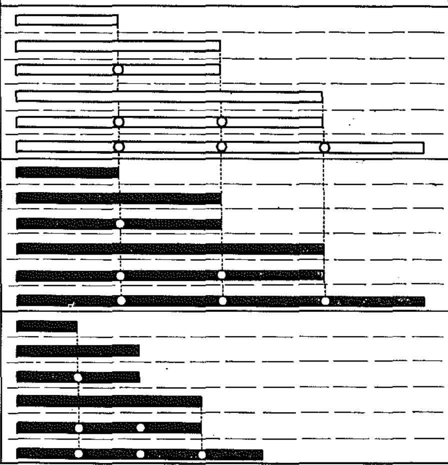	equal to W-Series in each designation	10.48 mm	circular drawn pipe	steel
	$2l$					
	$2\times l$					
	$3l$					
	$3\times l$					
	$4\times l$					
L	l			10.48 mm	circular solid bar	steel
	$2l$					
	$2\times l$					
	$3l$					
	$3\times l$					
	$4\times l$					
W	l		equal to P-Series in each designation	10.48 mm	circular solid bar	steel
	$2l$					
	$2\times l$					
	$3l$					
	$3\times l$					
	$4\times l$					

Rods of P-Series were made of steel pipe with an outside diameter 10.48 mm, whereas those of L and W-Series were made of round steel bar with the same diameter. When any discussion is made on the effects due to the types and properties of rods, the P-Series will always be taken as a standard, because a penetration rod in common use is not made of solid bar, but of steel pipe.

Rods of L-Series, when they have the same designation as P-Series, are of equal length to the P-Series, but differ in weight; for example the rod lengths of both P and L-Series with the same designation $3l$ are equally 299.4 cm, but the weight is 1,206 gr. for the P-Series and 2,020 gr. for the L-Series. From this, the effect on the measured strain at the end of the rod due to the weight of rod can be examined.

On the other hand, rods of W-Series are of equal weights to the P-Series, when the designations are common to both P and W-Series, but different in length; for example the length and weight of W-Series with the designation of $3l$ are 176.8 cm and 1,202 gr. respectively. This might indicate the effect due to the length of rod.

There are four lengths of rod in one Series, which are designated as l, $2l$, $3l$ and $4l$. Moreover there are 2 types of rod in one length for one Series of rod, for example $2l$ and $2\times l$, with the exception of the one assigned as standard with the designation l. The rod with the designation of $2l$ and $3l$ have no joints, and are in lengths 2 and 3 times the standard length l, whereas the rods of $2\times l$, $3\times l$ and $4\times l$ have several joints, but they are exactly the same as the corresponding jointless rods, except for the screw joints. From this, the author intended to examine some effects on the strain at the end of the rod due to the existence of joints.

Several rods are shown in Photo. 1; from left to right W. l, W. $2l$, W. $3l$, L. $2l$, P. l, P. $3\times l$ respectively, in which the first letter shows the series and the second shows the length of rod and whether the rod is jointed or not.

Test rods were supported by rod supports as shown in Photo. 2 at one to three points according to each length of rod to prevent transversal vibration and to hold the rods in an exactly vertical position. The part of a rod support which touched the rod was carefully made frictionless to permit a free vertical displacement for a rod during impact.

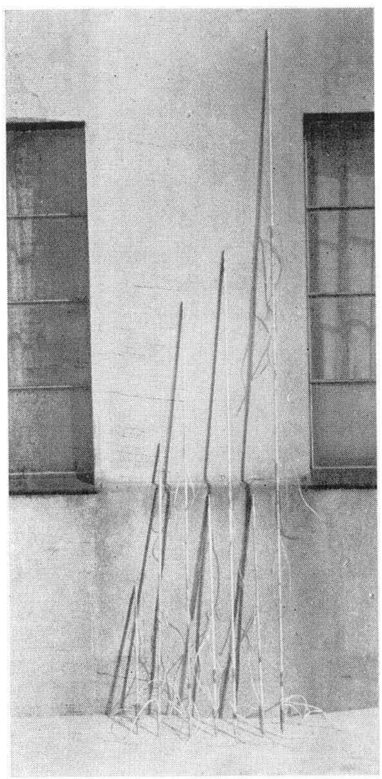

PhoGo. 1. Test rods.

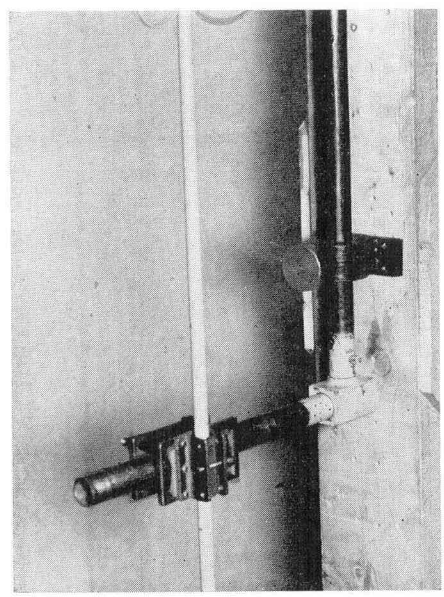

Photo. 2. Rod support.

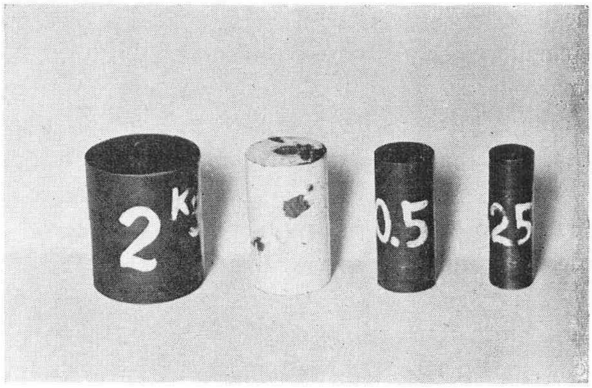

Photo. 3. Rammers.

(2) **Rammers and knocking head**

Four cylindrical rammers were prepared as shown in Photo. 3, whose weights were 0.25, 0.5, 1 and 2 kg. respectively, and their drop heights were varied every 10 cm from 10 to 50 cm, and were operated manually.

Photo. 4 shows the knocking head, whose guide rod and surface of contact with rammer were carefully made to make the impact by rammer transmit completely to the test rod.

The heights of these rammers were made equal for the convenience of their manipulation in which the operator dropped successively a rammer from the height of 10 cm to 50 cm, using the marks on the stem of the knocking head as a guide.

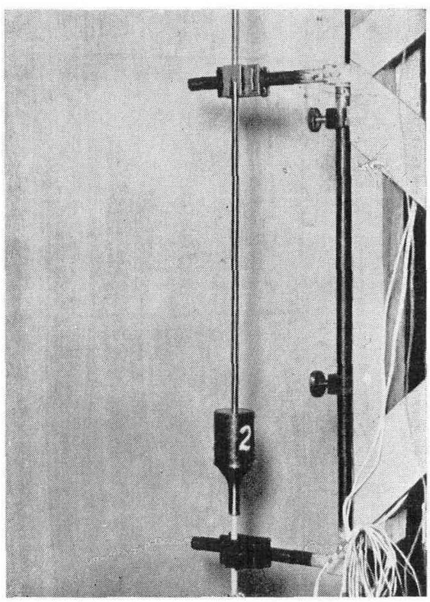

Photo. 4. Knocking head.

(3) **K-body**

The value of k, which is related to the mechanical property of the k-body, may be calculated as follows :

$$k=\frac{p}{EA}=\frac{1}{EA}\cdot\frac{E'A'}{l'}=\frac{E'}{E}\cdot\frac{A'}{A}\cdot\frac{1}{l'}$$

,where E', A' and l' are Young's modulus of elasticity, the sectional area and the length of the k-body respectively.

To make the value of k large, it is necessary either to increase the values of E' or A' of the k-body, or to decrease the values of E or A of the rod or the length of the k-body l'.

To make it small, E' or A' must be made small, or in another way E, A or l' must be made large. E and A, however, were fixed as stated before, since they are Young's modulus and the sectional area of the rod. Then E', A' and l' of the k-body are the only variables which can produce a value for k.

Two materials were selected as the k-body, one of which was a block of steel in a cylinderical form, whose modulus of elasticity was assumed to be 2.1×10^6 kg/cm². This was of course regarded as the larger value of k, which would correspond to firm foundation soil. The other material was a block of rigid polyvinyl chloride, whose Young's modulus was determined by a test as 8.4×10^4 kg/cm² as shown in Fig. 6. This material was intended to be a representative for a smaller value of k, which would correspond to soft foundation. Photo. 5 shows the k-bodies of all kinds mentioned above.

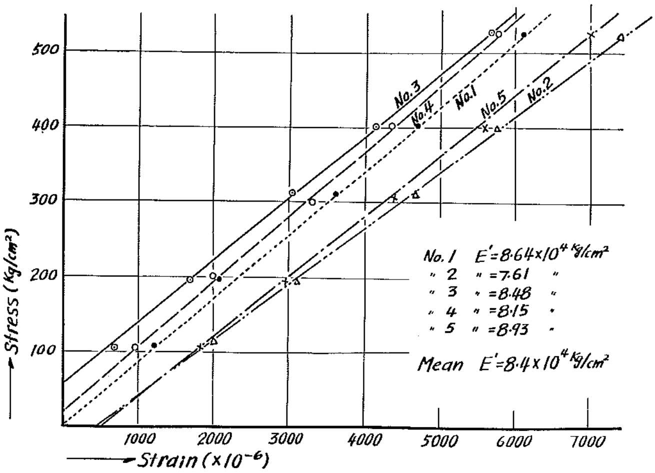

Fig. 6. Stress-strain curves for rigid polyvinyl chloride.

Referring to the sectional area of the k-body, it becomes difficult to analize the stress transmission from the end of the rod to the k-body, if the sectional area of the k-body is made much larger than that of the rod for obtaining a large value of k. On the other hand, it is not desirable to make it much smaller for the opposite purpose to the forgoing one on the value of k, the reason of which is that buckling in the k-body may happen and it was considered difficult to make such a slender block stand exactly vertical. To avoid these difficulties, the sectional area of the k-body A' was made equal to those of the rods for the L and W-Series, which was $A = A' = 0.863$ cm². The rods

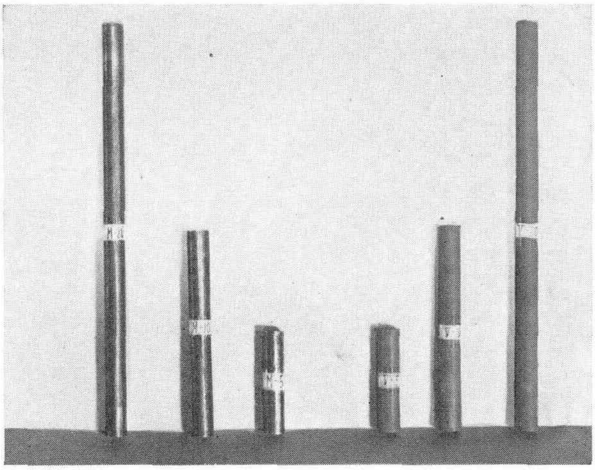

Photo. 5. k-bodies.

of the P-Series had different values of k from the other two varieties of rods for one kind of k-body, since their sectional area was different from the others.

As to the length of the k-body, three lengths of 5, 10, 20 cm were prepared. In general, a smaller value of k is more difficult to obtain than a larger one. For obtaining a smaller value of k, the length of the k-body must be large, which makes it difficult to let the k-body stand exactly vertical without any other helps. For practical purposes and convenience of the experimental equipment, these three lengths were chosen.

The k-body made of metal with 5 cm length was named M-5 and that of rigid polyvinyl chloride 10 cm in length was called V-10 and so on. The values of k for each k-body and rod are shown in Table 2.

TABLE 2. Values of k

Material	l' (cm)	P-Series	L, W-Series
Steel	20	0.050,15	0.085,79
	10	0.100,30	0.171,58
	5	0.200,60	0.343,16
Vinyl	20	0.002,00	0.003,42
	10	0.004,00	0.006,84
	5	0.008,00	0.013,69

The end of the rod was connected carefully to the k-body with a specially designed tool with an H shaped section, designated as H-body as shown in

Fig. 7. The thickness of the part of the H-body which connects the end of the rod with the top of the k-body was made as small as possible, so as not to disturb the transmission of strain and not to deviate from the assumed boundary conditions of elastic support. Photo. 6 shows the V–10 k-body and other equipment under test.

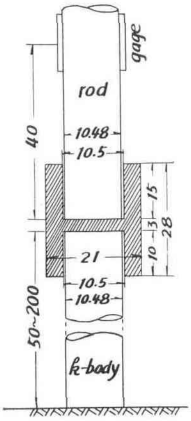

Fig. 7. H-body (unit in mm).

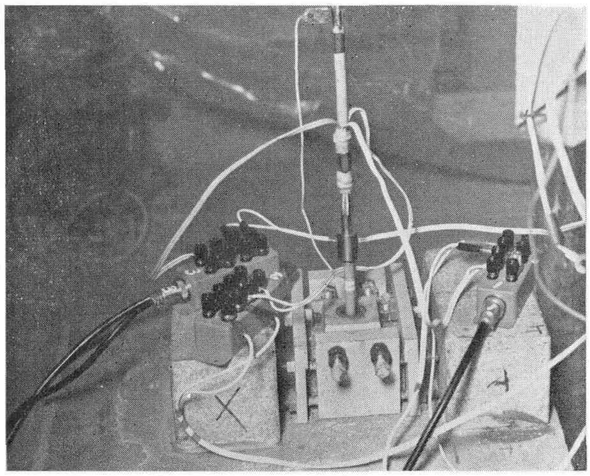

Photo. 6. k-body under test.

TABLE 3. Values of m and q for M–5

Series	Designation	k (cm^{-1})	l (cm)	kl	$G=2$ kg		$G=1$ kg		$G=0.5$ kg		$G=0.25$ kg	
					m	q	m	q	m	q	m	q
P	l	0.343	96.5	33.11	4.938	163.5	2.469	81.8	1.235	40.9	0.617	20.4
	$2l$	”	198.0	67.95	2.500	170.7	1.250	85.4	0.625	42.7	0.313	21.3
	$3l$	”	299.4	102.74	1.657	170.8	0.829	85.4	0.414	42.7	0.207	21.4
	$4l$	”	396.0	132.46	1.234	163.5	0.625	85.4	0.313	42.7	0.157	21.4
L	l	0.201	96.5	19.36	3.063	59.3	1.531	29.6	0.766	14.8	0.383	7.4
	$2l$	”	198.0	39.72	1.499	59.5	0.750	29.8	0.375	14.9	0.187	7.4
	$3l$	”	299.4	60.06	0.991	59.5	0.495	29.7	0.248	14.9	0.124	7.4
	$4l$	”	396.0	77.43	0.766	59.3	0.375	29.7	0.188	14.9	0.094	7.4
W	l	0.201	59.3	11.90	5.013	59.6	2.507	29.8	1.253	14.9	0.627	7.4
	$2l$	”	118.5	23.77	2.497	59.4	1.248	29.7	0.624	14.8	0.312	7.4
	$3l$	”	177.9	35.69	1.665	59.4	0.833	29.7	0.416	14.9	0.208	7.4
	$4l$	”	237.2	47.58	1.253	59.6	0.624	29.7	0.312	14.9	0.156	7.4

The values of q for every type of test rod and three types of k-body (M-5, M-20 and V-10), are shown in Table 3, 4 and 5 respectively, in which these three cases of k-body are repeatedly used in the following discussions of the test results.

TABLE 4. Values of m and q for M-20

Series	Designation	k (cm^{-1})	l (cm)	kl	G=2 kg		G=1 kg		G=0.5 kg		G=0.25 kg	
					m	q	m	q	m	q	m	q
P	l	0.086	96.5	8.28	4.938	40.9	2.469	20.4	1.235	10.2	0.617	5.1
	$2l$	"	198.0	16.99	2.500	42.7	1.250	21.3	0.625	10.7	0.313	5.3
	$3l$	"	299.4	25.69	1.657	42.7	0.829	21.4	0.414	10.7	0.207	5.3
	$4l$	"	396.0	33.11	1.234	40.9	0.625	21.4	0.313	10.7	0.157	5.3
L	l	0.050	96.5	4.84	3.063	14.8	1.531	7.4	0.766	3.7	0.383	1.9
	$2l$	"	198.0	9.93	1.499	14.9	0.750	7.4	0.375	3.7	0.187	1.9
	$3l$	"	299.4	15.01	0.991	14.9	0.495	7.4	0.248	3.7	0.124	1.9
	$4l$	"	396.0	19.36	0.766	14.8	0.375	7.4	0.188	3.7	0.094	1.9
W	l	0.050	59.3	2.97	5.013	14.9	2.507	7.4	1.253	3.7	0.627	1.9
	$2l$	"	118.5	5.94	2.497	14.8	1.248	7.4	0.624	3.7	0.312	1.9
	$3l$	"	177.9	8.92	1.665	14.9	0.833	7.4	0.416	3.7	0.208	1.9
	$4l$	"	237.2	11.90	1.253	14.9	0.624	7.4	0.312	3.7	0.156	1.9

TABLE 5. Values of m and q for V-10

Series	Designation	k (cm^{-1})	l (cm)	kl	G=2 kg		G=1 kg		G=0.5 kg		G=0.25 kg	
					m	q	m	q	m	q	m	q
P	l	0.007	96.5	0.661	4.938	3.26	2.469	1.63	1.235	0.816	0.617	0.408
	$2l$	"	198.0	1.356	2.500	3.39	1.250	1.70	0.627	0.848	0.313	0.425
	$3l$	"	299.4	2.051	1.657	3.39	0.829	1.70	0.414	0.849	0.207	0.425
	$4l$	"	396.0	2.644	1.234	3.26	0.625	1.65	0.313	0.828	0.157	0.415
L	l	0.004	96.5	0.386	3.063	1.18	1.531	0.59	0.766	0.296	0.383	0.148
	$2l$	"	198.0	0.792	1.499	1.19	0.750	0.59	0.375	0.297	0.187	0.148
	$3l$	"	299.4	1.198	0.991	1.19	0.495	0.59	0.248	0.297	0.124	0.149
	$4l$	"	396.0	1.544	0.766	1.18	0.375	0.58	0.188	0.290	0.094	0.145
W	l	0.004	59.3	0.237	5.013	1.19	2.507	0.59	1.253	0.298	0.627	0.149
	$2l$	"	118.5	0.474	2.497	1.18	1.248	0.59	0.624	0.296	0.312	0.148
	$3l$	"	177.9	0.712	1.665	1.19	0.833	0.59	0.416	0.297	0.208	0.148
	$4l$	"	237.2	0.949	1.253	1.19	0.624	0.59	0.312	0.296	0.156	0.148

(4) **Base material**

In the introduction of the fundamental equations, it was assumed that the k-body should stand on rigid material in which no deformation might occur. It follows that the material on which the k-body stands should have an infinite modulus of elasticity, but such material can seldom or never be found. At the same time it should have a comparatively large mass to resist impact and to show no displacement. Two materials, stone ($10 \times 10 \times 6\ cm^3$, granite) and hard steel (equal in size to stone, carbon content 0.6%) were chosen for this purpose, since it was found difficult and expensive to prepare such a material that had a much higher degree of elasticity than steel and in addition had a sufficient mass. (Photo. 7 and 8).

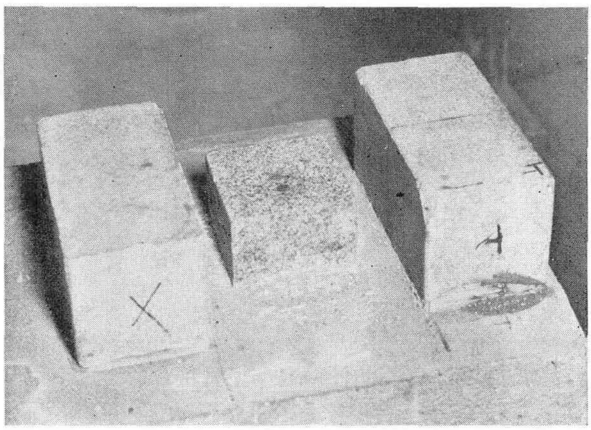

Photo. 7. Stone base.

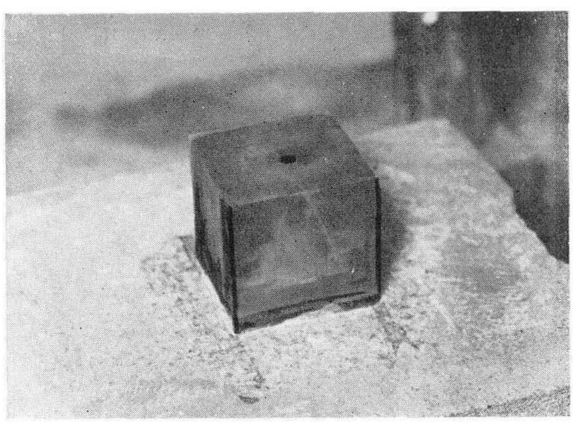

Photo. 8. Steel base.

These base materials were fixed by certain epoxy resin, making their surface completely smooth and horizontal upon a massive stone of andesite, $37 \times 51 \times 26$ cm^3 in size and about 150 kg in weight. This andesite was expected to add mass to the base materials and was cemented to a rigid floor of the laboratory.

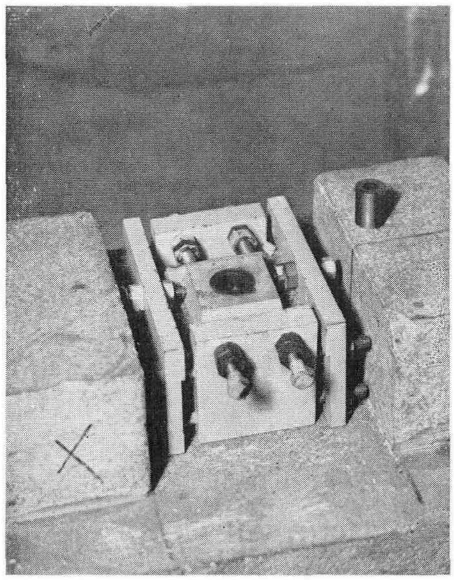

Photo. 9. k-body holder and H-body.

The test on the stone base was named A-Test and that on the steel base was called B-Test. Granite is lower than steel in modulus of elasticity by one tenth to one third. It might naturally be expected that the test results of the B-Test should be larger than those of the A-Test, because the boundary conditons of the experiment in the B-Test were closer than the A-Test to the assumed condition, even though by a little amount. It might also be presumed that much smaller values of strain would be obtained in the A and B Tests than those calculated theoretically. These losses or discrepancies partly due to the condition of the basement will be discussed later in detail.

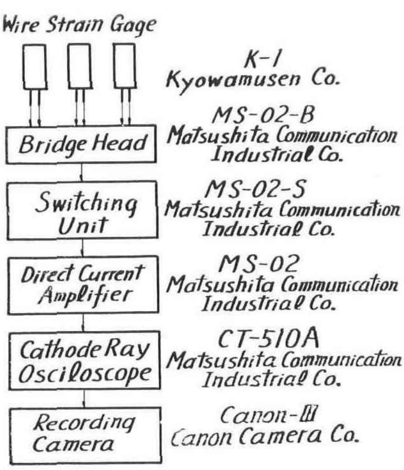

Fig. 8. Schematic diagram for measuring equipment.

The k-body was made to stand precisely vertical by two transits set roughly at right angles and was situated exactly on the base material by an adjustable k-body holder as seen in Photo. 9.

(5) Strain measurement

Fig. 8 shows a schematic diagram for the measuring equipment of impact strain which consists mainly of a wire strain-meter set and a cathode ray osciloscope. There are some other methods of measuring impact strain 4), 5), but the above mentioned instruments were decided upon, since they were not difficult either to prepare or to operate and furthermore they could be kept in good working condition as they were operated only in the laboratory, where the air was rather dry and the temperature did not change much during the test.

Strain gage

As seen in every reference book in elasticity, the frequency of the longitudinal vibration is $a/2l$ in the impact of a rod, one end of which is freely supported and struck longitudinally on the other, whereas it becomes $a/4l$ when the rod is fixed at one end instead of the free support. In the present problem of the elastic support, the frequency may be estimated to vary from $a/2l$ to $a/4l$.

The propagation velocity a of elastic longitudinal waves has approximately a value of 5,000 m/sec for steel and the length of the shortest test rod in this experiment was 59.3 cm of unit length l in the W-Series. Then the maximum frequency in this test might be calculated as 2,170 to 4,330 cps.

The strain gages used in this experiment were K–1 by the Kyowamusen

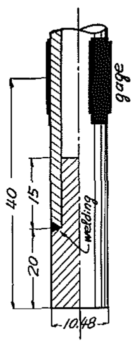

Fig. 9. Position of gage at rod end. (P-Series, the same for L, W-Series, unit in mm)

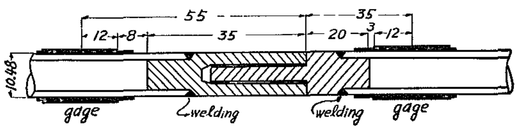

Fig. 10–1. Position of gage at intermediate point. (P-Series, unit in mm)

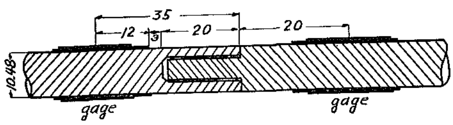

Fig. 10–2. Position of gage at intermediate point. (L, W-Series, unit in mm)

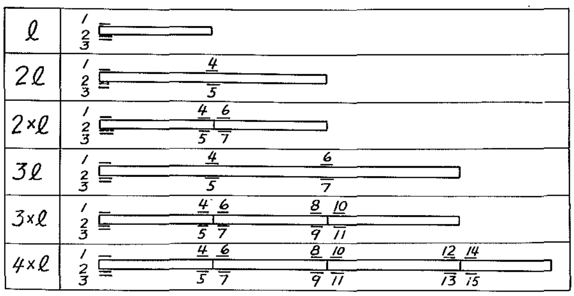

Fig. 11. Names and number of gages for each rod.

Co. with a length of 1.95 cm, a resistance of 120 Ω, a factor of 2 and a paper base. A strain gage with a paper base is said to have enough fidelity to vibration frequencies up to 50 to 100 Kcps 6), 7), hence this type of strain gage may be regarded as having sufficient ability in turning the strain exerted by the longitudinal impact into unbalanced electric voltage.

Fig. 9, 10 and 11 show the details of the positions, names and the number of these strain gages which were applied to each rod. The strain gages of No. 1, 2 and 3 by which the strains at the end of the rod were intended to be measured, could not be adhered to the real end, as seen in Fig. 9. This made it necessary to convert the strain measured by the existing gages to the sought-after strain at the real end. For this purpose, the theoretical strains at the points where the gages were adhered, were calculated for various combinations of m and q by the equations (2) to (7) and comparing these values with the theoretical ones at the end, the coefficients of correction for all the rod series and the k-bodies were obtained as shown in Table 6. A measured strain multiplied by a corresponding value in Table 6 would give the amount to be added to it to acquire the real strain at the end. The variations of these coefficients according to the values of m and q are very interesting, but they were not included in the present paper, because it was considered that they had no direct relations to this investigation.

The strain gages at the intermediate points were used to examine the effect of the joint on the strain to be measured at the end of the rod. The intermediate points of adherence in the P-Series were placed slightly farther apart from the joint than those in the other two series to avoid the welded part of the screw joint as shown in Fig. 10-1.

At the end of the rod, three strain gages were set, whereas only two were used at the intermediate points of the rod, the reason of which was that the strains exerted at the rod end were far more inportant than those at the intermediate points in the present investigation. The strains were measured independently by each set of gages at one position of the rod and the mean values were taken.

Bridge head and switching unit

Bridge head (Photo. 10) was a Wheatstone type for DC current and the 2-gage-method with a dummy gage was applied to remove the effect of temperature.

As shown in Photo. 11 (second from the right), a switching unit was used for connecting strain gage and strainmeter to each other continuously with 8 elements.

TABLE 6. Coefficients of Correction (in %)

Series	Designation	Metal k-body												Vinyl k-body											
		M-20				M-10				M-5				V-20				V-10				V-5			
		Rammer weight (kg)												Rammer weight (kg)											
		2	1	0.5	0.25	2	1	0.5	0.25	2	1	0.5	0.25	2	1	0.5	0.25	2	1	0.6	0.25	2	1	0.5	0.25
P	l	1.9	2.5	3.4	6.8	1.9	3.6	3.5	7.0	1.9	3.8	6.0	7.4	1.0	1.7	3.1	3.6	1.2	1.8	3.2	5.3	1.5	2.0	3.3	5.8
	$2l$	1.8	1.8	3.5	6.3	1.9	3.0	3.5	6.4	2.0	4.2	3.5	6.4	0.9	1.6	2.5	2.1	1.0	1.6	2.9	3.4	1.0	1.7	2.2	4.7
	$3l$	2.1	1.6	3.2	5.9	2.2	1.7	3.2	5.9	2.2	1.7	3.3	6.0	0.7	1.3	2.1	1.4	0.8	1.4	2.6	2.3	0.8	1.4	3.0	4.1
	$4l$	1.5	1.7	3.2	6.1	2.1	1.8	3.2	6.6	2.3	1.8	3.3	6.6	0.8	1.4	1.7	1.1	0.8	1.7	2.3	1.8	0.9	1.7	2.9	3.3
L	l	2.2	2.7	5.1	9.9	2.7	3.8	4.8	10.7	3.6	5.9	5.0	10.5	1.4	2.5	2.7	1.4	1.6	2.5	3.6	3.3	1.8	2.6	4.4	5.8
	$2l$	2.1	2.7	5.0	8.9	2.8	2.8	5.1	9.9	3.5	2.7	5.6	10.3	1.2	1.9	1.6	0.7	1.2	2.1	2.8	1.6	1.3	2.3	3.8	2.8
	$3l$	1.3	2.8	5.0	6.9	1.7	2.8	5.1	8.3	1.7	2.8	5.2	9.8	1.0	1.3	1.0	0.4	1.2	2.1	1.8	1.0	1.2	2.4	3.0	1.8
	$4l$	1.3	2.6	4.9	5.8	1.4	2.7	5.0	7.5	1.3	2.5	5.1	9.3	1.1	1.4	0.8	0.3	1.2	1.9	1.4	0.8	1.3	2.3	2.5	1.5
W	l	2.7	3.6	5.6	10.1	2.9	3.8	5.6	11.2	3.4	5.0	5.6	11.5	1.2	2.5	3.6	2.2	1.6	2.7	4.7	4.6	2.0	2.9	5.1	4.9
	$2l$	1.9	3.6	5.7	10.1	2.6	2.9	6.0	10.5	3.2	4.1	5.6	10.8	1.4	2.4	2.4	1.1	1.5	2.7	3.6	2.7	1.6	2.6	4.8	4.8
	$3l$	1.9	2.8	5.1	9.6	3.1	2.6	5.3	9.9	3.7	2.8	5.3	10.0	1.2	1.9	1.7	0.7	1.2	2.2	3.0	1.8	1.2	2.3	4.1	3.1
	$4l$	1.4	3.0	5.2	8.2	2.0	2.9	5.4	9.6	3.2	3.4	5.4	11.0	1.3	1.9	1.3	0.6	1.4	2.4	2.4	1.3	1.4	2.6	3.5	2.2

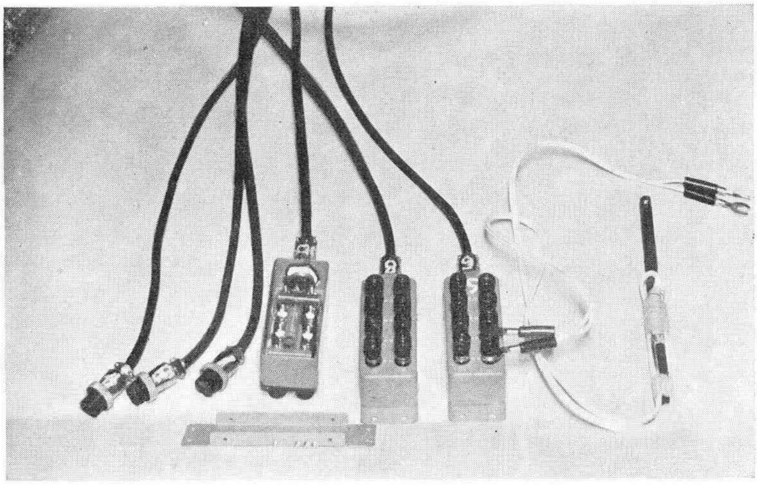

Photo. 10. Bridge heads.

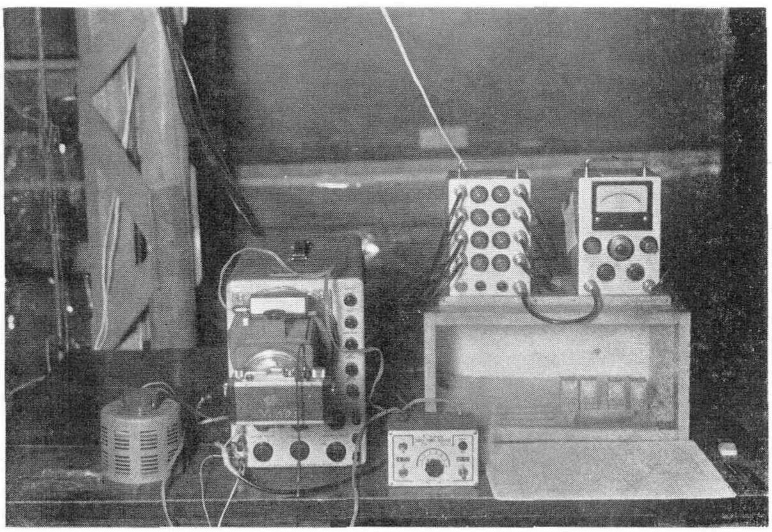

Photo. 11. Measuring apparatus.

Strainmeter and cathode ray oscilloscope

A strainmeter MS-02 made by the Matsushita Communication Industrial Co. was used, the specifications of which shows ;

1) range of strain measured 1 or 3 to $10{,}000 \times 10^{-6}$
2) accuracy 3×10^{-6}
3) frequency characteristics DC to 10 kc (—3 db)
4) amplification 32 db

The range of the theoretical strain from the impact was calculated as 1.0 to $3.3\times V/a$, which would reach 280 to $2{,}100\times10^{-6}$ when the propagation velocity a was assumed to be approximately 5,000 m/sec and the rammer velocity V at the instant of impact was considered to be 1.4 to 3.1 m/sec for 10 to 50 cm drop heights of the rammer, based roughly on the formula of $\sqrt{2gH}$. If the strain to be created should decrease to 1/4 of the theoretical value due to various losses, the range of strains to be measured would be 70 to 500×10^{-6} and so the MS-02 strainmeter was regarded as sufficient for the purpose of this strain measurement in its sensitivity and range.

The fidelity to the vibration frequency of this strainmeter could also be considered as sufficient for this test as discussed previously. The MS-02 strainmeter is shown on the right in Photo. 11.

The specification of the cathode ray oscilloscope CT-510A by the same manufacturer was as follows;

1)	sensitivity of the maximum vertical deflection	0.01 Vdc/cm
2)	frequency characteristics	DC to 50 kc (—3 db)
3)	screen diameter	130 mm
4)	sweep range	1 sec/cm to 0.3 μ sec/cm

It is shown in Photo. 11 (the third from the right, with the recording camera). The most important points of interest in this apparatus were that this oscilloscope had a high sensitivity in vertical deflection and was equipped with a DC amplifier as was in the case of the MS-02 strainmeter.

Recording Camera

A Canon III Camera and X-ray 35 mm film were used. The photo-oscilloscope unit CO-133-W by the Canon Camera Co. was also used as shown in Photo. 11 and was found to be highly satisfactory.

The view of the complete apparatus is shown in Photo. 12.

(6) Method of observation

The knocking head, test rod and k-body were so made as to stand exactly vertical by the two engineering transits as mentioned before. Strain gages, bridge heads, switching unit, MS-02 strainmeter, CT-510A cathode ray oscilloscope and camera were properly connected and carefully adjusted. Whereupon a certain known strain was inserted into the oscilloscope by appropriate manipulation of the strainmeter, which was recorded as shown in Photo. 13-

The magnitude of this calibrating strain was decided so as to be slightly larger than the expected maximum strain in one set of the tests, which were found by the trial test on the largest drop height.

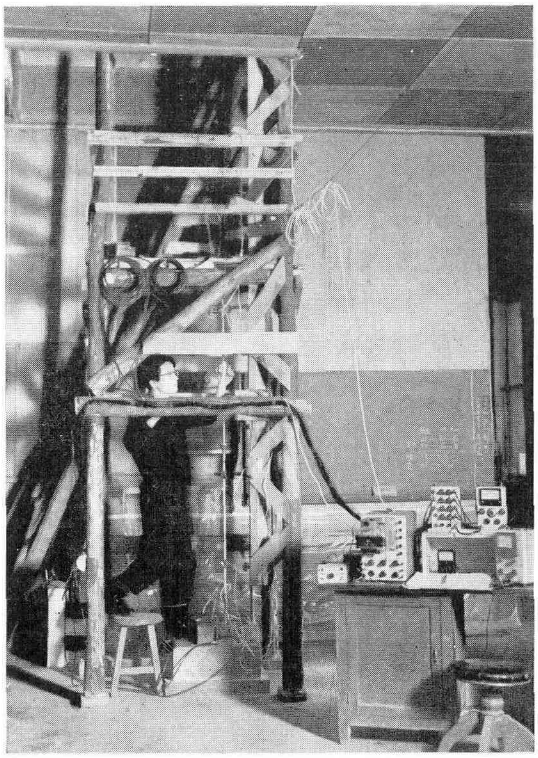

Photo. 12. View of complete apparatus.

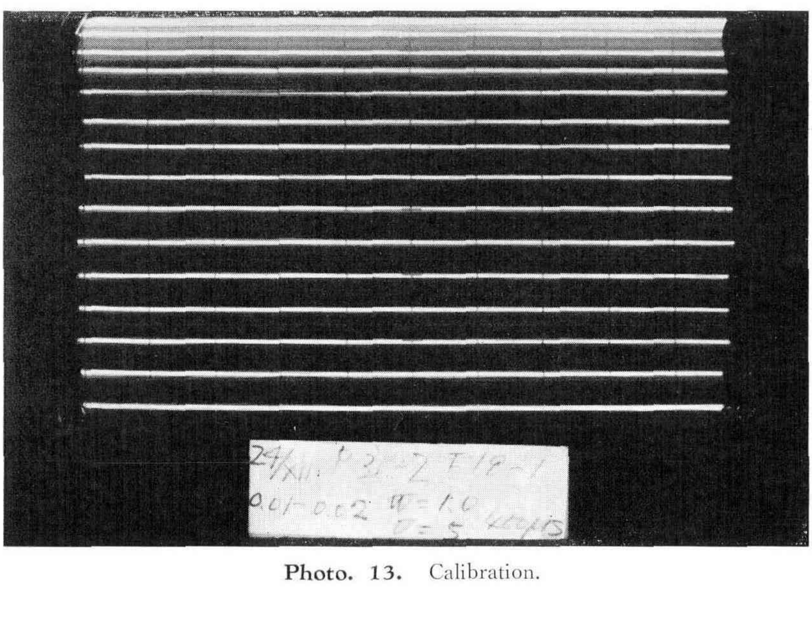

Photo. 13. Calibration.

For one gage, the rammer was continously dropped 15 times by manual operation, at the rate of 3 rounds of 5 blows each, in which one round was initiated at $H=10$ cm and terminated at $H=50$ cm, during which the camera was left open. The sweep range of the oscilloscope was so adjusted that the vertical deflections exerted by the above mentioned 15 blows were completely caught in one film. Each deflection by one blow did not have a curve for strain-time such as those in Fig. 3, but rather a single vertical line. The curved line corresponding to each condition of impact might be obtained, if the oscilloscope spot should properly be swept so as to coincide with the frequency of the longitudinal elastic wave, but it was not necessary to determine the exact vibration curves, because the present purpose of the investigation was to measure any maximum compressive strain both at the end and at the intermediate point of the rod under various conditions of impact. This method of measurement has saved much time and expenditure.

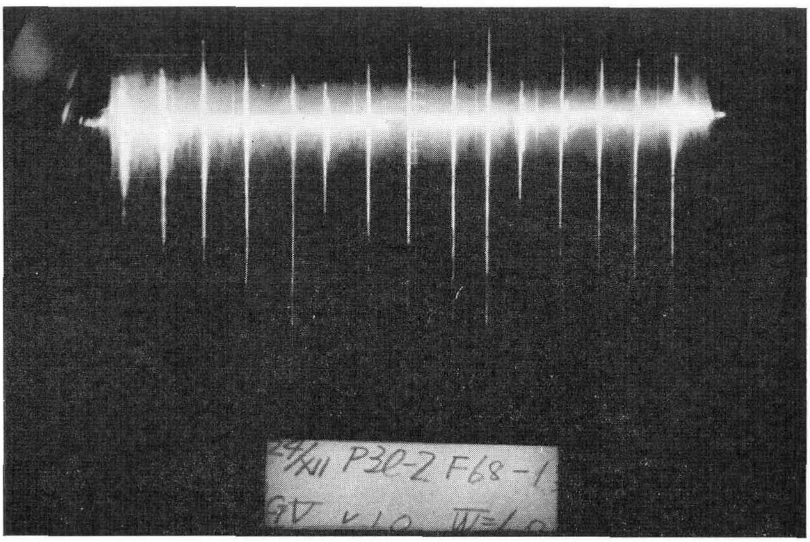

Photo. 14. Camera record.

The 15 vertical lines in the lower part of Photo. 14 were the electric signals proportional to compressive impact strains created in the rod, which made it possible to determine the magnitudes of strain by both measuring their lengths from the horizontal zero line which can be seen on the brilliant band in Photo. 14, and comparing these with that from Photo. 13, in which the magnitude of strain was known.

At the end of the rod, strains were observed by 3 gages in regular order as stated before, and thus at least 9 values of strain were obtained for one height of the rammer drop, while 6 values were taken by 2 gages at the intermediate point.

The microreader in Photo. 15 had been used for measuring the deflecting length of the spot from the zero line, in which the magnifying ratio was about 2.5 times and it was ascertained that the instrument did not produce any distorted projection.

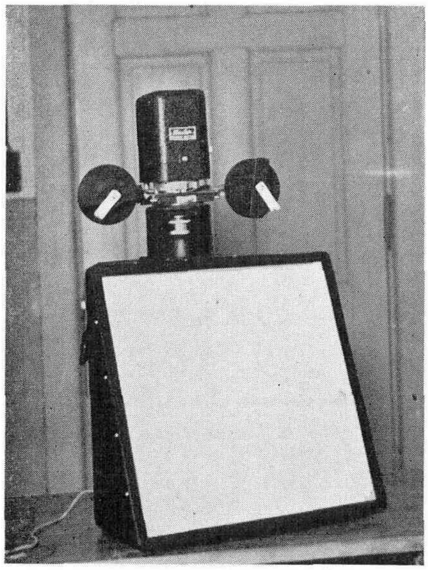

Photo. 15. Microreader.

2. Test Results

Some of the test results are shown in Table 7 to 12. Those for the end of the rod on both $2l$, $3\times l$, $4\times l$ of the A-Test and $2\times l$, $3\times l$ of the B-Test were omitted, and those for the intermediate point on $3l$, $3\times l$, $4\times l$ of the A-Test were not shown.

In the test of the rod length l and $3l$ for both A and B Tests, the sign of infinity (∞) in the column of the k-body means that in this case the k-body was removed and the rod was made to stand directly on the base material of stone or metal. This method of test should correspond to the boundary condition of impact for the fixed end, but it was considered that the elastic properties of the base materials, together with the foundation of the larger block of andesite and the concrete floor, might not be sufficient for the purpose of this experiment. Thus the test results of this method could be expected to be relatively larger than those by the ordinal tests with k-bodies.

TABLE 7. Test Results, l, Rod End, A-Test, $(\times 10^{-6})$

Series	k-body	G=0.25 kg H (cm)					G=0.5 kg H (cm)					G=1 kg H (cm)					G=2 kg H (cm)				
		10	20	30	40	50	10	20	30	40	50	10	20	30	40	50	10	20	30	40	50
P	∞	138	181	226	257	283	182	265	294	335	401	254	307	387	458	520	374	510	632	748	806
	M- 5	122	166	197	221	237	178	256	278	317	376	237	334	418	486	535	340	483	610	708	779
	M-10	105	147	179	209	227	151	224	256	306	335	224	311	396	484	530	323	479	600	678	765
	M-20	92	132	161	199	225	148	194	246	280	320	211	326	387	448	504	321	460	587	653	743
	V- 5	76	126	155	167	186	111	151	206	246	267	177	246	300	316	363	228	288	350	398	438
	V-10	77	97	124	154	173	95	138	178	203	229	148	201	256	306	346	194	294	347	380	431
	V-20	74	88	104	120	135	91	123	150	169	192	147	190	243	269	276	176	216	301	383	389
L	∞	125	167	212	252	281	143	200	248	306	343	190	302	362	434	476	282	441	500	591	670
	M- 5	93	128	152	171	188	125	170	206	229	251	179	250	322	375	434	247	358	443	496	550
	M-10	79	116	132	142	170	112	156	180	208	233	160	207	264	325	383	225	332	424	440	516
	M-20	72	103	119	135	143	99	126	153	184	205	146	185	245	302	352	206	316	400	415	452
	V- 5	55	75	91	106	116	77	107	141	182	198	132	188	248	294	338	182	253	290	334	359
	V-10	54	71	90	103	114	84	117	141	158	158	105	163	209	236	247	164	196	240	275	288
	V-20	53	72	76	99	112	71	98	110	127	141	100	134	171	202	236	148	188	219	240	275
W	∞	117	166	201	242	273	146	218	268	294	334	180	300	352	422	437	328	449	555	665	717
	M- 5	83	112	142	161	182	128	154	195	222	240	191	295	322	370	422	304	432	555	660	698
	M-10	78	106	129	148	163	118	160	198	219	266	177	262	312	364	406	277	394	454	562	594
	M-20	74	102	122	140	153	113	151	185	224	264	165	257	306	350	393	261	365	434	490	559
	V- 5	68	89	115	131	155	97	140	170	195	224	146	204	260	300	332	204	292	369	397	491
	V-10	61	84	108	129	145	99	130	160	186	220	142	175	233	265	290	181	268	336	359	425
	V-20	53	74	91	104	120	86	106	141	168	198	131	181	225	245	282	169	224	304	344	386

TABLE 8. Test Results, $3l$, Rod End, A-Test, $(\times 10^{-6})$

Series	k-body	G=0.25 kg H (cm)					G=0.5 kg H (cm)					G=1 kg H (cm)					G=2 kg H (cm)				
		10	20	30	40	50	10	20	30	40	50	10	20	30	40	50	10	20	30	40	50
P	∞	123	168	200	230	259	172	245	265	271	276	165	242	322	326	356	250	258	399	419	442
	M- 5	111	149	175	194	212	139	188	207	244	285	150	242	280	325	374	212	309	381	428	485
	M-10	77	112	128	146	159	134	182	188	226	250	136	204	248	298	320	179	302	368	414	483
	M-20	72	99	119	135	152	112	140	176	202	218	132	196	252	298	327	195	274	334	336	421
	V- 5	54	74	97	110	127	91	105	141	151	169	100	145	184	208	229	168	214	268	312	346
	V-10	51	73	95	100	122	75	103	128	150	168	106	134	157	176	203	153	204	242	301	339
	V-20	53	74	90	106	118	75	98	127	145	163	90	123	149	178	204	143	196	255	304	341
L	∞	128	173	212	242	270	131	184	222	258	282	136	191	238	276	316	181	259	311	361	402
	M- 5	86	123	149	174	194	106	153	185	209	231	115	173	214	255	288	168	232	293	338	386
	M-10	81	112	133	152	166	103	143	177	204	221	108	165	204	235	284	159	225	282	331	368
	M-20	67	89	107	120	133	92	132	164	181	203	105	157	198	216	251	144	199	258	294	337
	V- 5	44	62	75	87	96	55	82	102	119	132	92	121	149	162	179	116	167	210	248	266
	V-10	45	62	76	88	95	64	82	99	118	129	76	107	142	153	168	114	144	170	206	238
	V-20	45	63	76	88	98	54	78	95	108	118	77	109	132	150	160	107	140	175	192	226
W	∞	127	173	214	245	270	156	210	249	286	325	187	259	324	366	396	227	295	375	416	468
	M- 5	81	121	150	173	187	125	179	210	242	262	163	234	268	310	350	197	280	355	390	417
	M-10	71	106	127	141	158	104	146	171	193	202	139	186	236	261	292	181	271	326	367	389
	M-20	61	86	104	117	134	90	127	155	166	194	134	176	191	231	264	171	257	292	341	367
	V- 5	50	76	88	98	116	78	111	128	148	167	118	148	171	195	208	143	184	214	258	273
	V-10	49	69	78	90	110	77	107	128	149	164	107	132	161	184	200	133	177	210	240	258
	V-20	50	66	80	86	105	75	97	116	135	149	102	127	155	178	196	133	170	199	238	255

TABLE 9. Test Results, $2\times l$, Intermediate Point, A-Test, $(\times 10^{-6})$

Series	k-body	Mean values from gage No. 4 and 5										Mean values from gage No. 6 and 7									
		$G=0.25$ kg H (cm)					$G=1$ kg H (cm)					$G=0.25$ kg H (cm)					$G=1$ kg H (cm)				
		10	20	30	40	50	10	20	30	40	50	10	20	30	40	50	10	20	30	40	50
P	M- 5	66	89	106	125	143	169	240	317	356	384	70	92	124	157	182	166	238	289	327	376
	M-10	60	84	103	122	139	164	235	291	323	369	76	102	126	151	168	169	230	288	328	342
	M-20	58	80	100	119	139	163	222	282	314	354	74	98	124	150	168	138	205	225	280	324
	V- 5	62	88	110	124	135	133	175	215	265	322	64	87	108	121	136	140	221	249	279	301
	V-10	62	80	98	114	128	120	160	210	258	292	63	92	109	126	137	126	188	222	269	287
	V-20	62	81	98	111	126	110	154	209	253	280	60	84	102	118	132	127	167	204	225	252
L	M- 5	48	72	87	96	114	124	187	242	305	331	61	84	97	106	128	147	186	216	251	282
	M-10	64	88	108	128	152	127	184	242	280	317	50	75	88	98	109	138	183	213	242	275
	M-20	60	86	106	125	144	125	184	222	254	291	53	69	83	94	105	135	202	265	288	311
	V- 5	57	87	100	113	128	116	158	192	208	230	55	74	89	98	118	124	166	209	222	247
	V-10	54	78	95	113	118	98	131	168	187	204	54	68	82	96	115	116	139	181	198	220
	V-20	52	73	88	111	118	91	128	151	183	200	51	71	95	108	114	110	128	178	197	246
W	M- 5	54	77	93	106	120	157	235	273	317	372	58	79	100	119	136	150	220	267	329	367
	M-10	54	72	93	109	120	145	214	257	300	357	53	76	95	110	128	151	217	267	315	349
	M-20	53	68	84	96	123	143	201	245	287	322	50	78	104	117	130	140	207	245	296	330
	V- 5	52	68	86	102	114	141	191	206	239	287	58	83	100	122	142	127	158	173	192	244
	V-10	58	75	85	99	112	122	165	180	237	264	60	85	109	125	136	105	140	161	177	210
	V-20	53	75	91	99	115	115	143	174	203	218	50	74	89	99	113	103	136	158	167	199

TABLE 10. Test Results, l, Rod End, B-Test, ($\times 10^{-6}$)

Series	k-body	G=0.5 kg H (cm) 10	20	30	40	50	G=1 kg H (cm) 10	20	30	40	50	G=2 kg H (cm) 10	20	30	40	50
P	∞	195	268	339	388	419	228	304	414	499	567	389	537	644	726	802
	M- 5	185	264	300	347	384	237	353	439	484	545	338	508	630	716	780
	M-20	149	212	253	302	324	224	327	398	454	509	333	479	551	681	762
	V-10	123	184	205	222	234	163	216	264	329	365	242	309	349	419	468
L	∞	172	238	297	352	393	220	294	367	418	476	302	444	565	667	828
	M- 5	140	189	239	270	315	187	261	328	385	446	285	381	456	547	621
	M-20	117	158	191	212	240	169	226	274	312	366	246	360	402	476	546
	V-10	97	129	153	169	200	142	205	243	284	309	229	308	353	441	504
W	∞	163	226	277	302	329	307	396	494	543	600	392	563	724	837	946
	M- 5	133	190	227	254	281	208	302	351	428	501	393	513	559	677	750
	M-20	109	152	184	216	235	192	268	320	359	413	304	398	488	565	611
	V-10	110	147	177	209	244	164	220	257	303	347	190	255	317	354	376

TABLE 11. Test Results, $2l$, Rod End, B-Test, ($\times 10^{-6}$)

Series	k-body	G=0.5 kg H (cm) 10	20	30	40	50	G=1 kg H (cm) 10	20	30	40	50	G=2 kg H (cm) 10	20	30	40	50
P	M- 5	174	243	290	318	339	198	274	318	352	382	270	388	482	554	620
	M-20	162	215	250	276	305	176	251	291	319	336	261	363	432	486	559
	V-10	106	145	168	193	206	163	219	239	257	284	184	291	351	395	414
L	M- 5	149	212	256	286	303	183	264	314	347	382	225	315	385	442	500
	M-20	111	153	174	203	222	155	216	252	286	311	190	272	328	398	432
	V-10	78	108	133	162	176	128	157	186	196	209	148	181	221	248	285
W	M- 5	142	207	248	271	280	173	260	308	340	355	262	373	450	536	594
	M-20	125	174	203	216	222	150	229	269	299	320	208	296	370	462	515
	V-10	105	158	188	199	214	140	188	209	253	279	161	210	263	292	338

TABLE 12. Test Results, $3l$, Rod End, B-Test, ($\times 10^{-6}$)

Series	k-body	$G=0.5$ kg H (cm)					$G=1$ kg H (cm)					$G=2$ kg H (cm)				
		10	20	30	40	50	10	20	30	40	50	10	20	30	40	50
P	∞	221	288	343	392	431	208	272	376	401	452	270	347	430	468	556
	M- 5	153	214	259	288	318	188	256	321	380	416	215	316	383	433	490
	M-20	132	172	197	216	242	147	208	282	316	346	209	286	343	376	418
	V-10	96	124	148	169	187	106	141	168	189	207	159	239	277	323	344
L	∞	172	244	300	356	406	168	233	272	344	389	219	293	348	417	433
	M- 5	148	209	257	301	321	139	198	247	295	326	175	253	307	352	370
	M-20	113	153	181	203	218	143	187	231	263	293	159	220	272	307	330
	V-10	65	101	123	147	163	85	112	144	164	185	125	146	187	225	255
W	∞	175	242	292	338	370	214	285	310	372	413	244	354	503	551	612
	M- 5	136	199	230	262	289	154	227	285	332	364	207	299	366	410	472
	M-20	99	138	163	186	211	136	197	234	273	296	195	270	326	366	422
	V-10	77	110	136	156	178	130	163	212	234	278	168	211	264	296	330

In the test of B, the rammer with 0.25 kg weight and the k-bodies of M-10, V-5, V-20 were not used, and moreover the measurements were not made on all the intermediate points of the rods, because the B-Test was only aimed to ascertain what better conditions of the base material might yield a larger strain than the other, which could be one of the verifications for the correctness of the fundamental equations.

3. Discussion of Test Results

(1) Drop height

The fundamental equations from (8) to (11) for the maximum strain at the end of the rod are always accompanied with the term V which is the rammer velocity at the instant of impact. When the rammer is dropped from the height of H, V may approximately be assumed to be $\sqrt{2gH}$. Then it can be considered that the maximum strain at the end of the rod should not be proportional to H as usually indicated in the existing dynamic pile driving formulas, but rather to the square root of H. The observed strain for 5 drop heights should make a straight line and pass through the origin of the coordinate, when plotted to the square root of H.

Fig. 12 and 13 show some of the relations between the observed strain

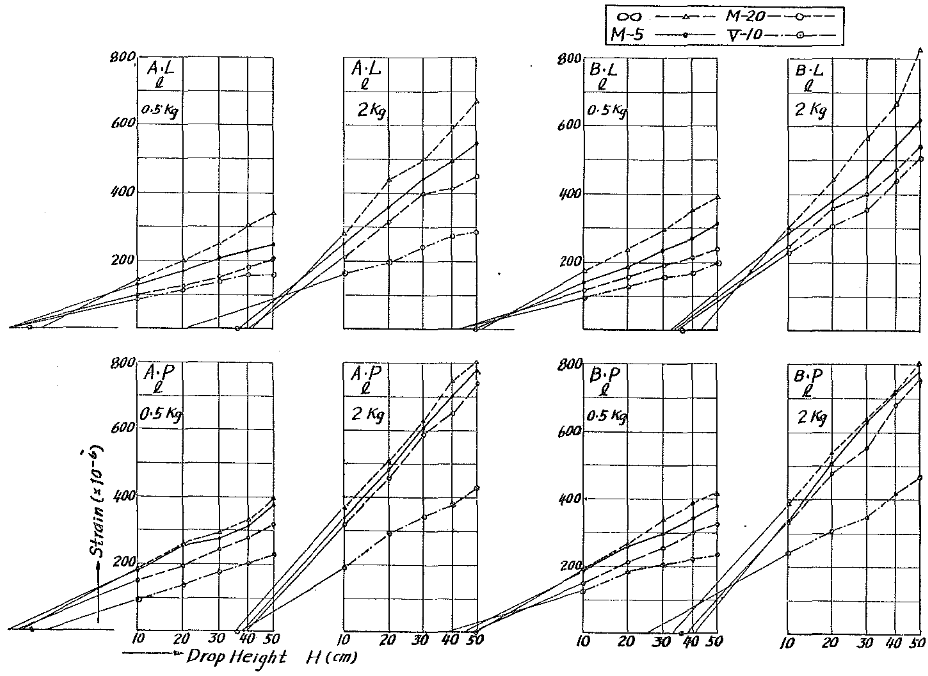

Fig. 12. Strain-$\sqrt{H}$ curves (l).

and the square root of the drop height, in which A and B are the type of test, while P, L, and W are the designations of the test rod. l and $3l$ stand for their length, and kg shows the weight of the rammer. In these figures, straight lines were fitted so as to pass through every plotted point as far as possible by approximate estimation and this seemed to have been satisfactory and successful except in several examples, but these lines were not drawn to avoid the confusion of the figures. These lines were at the same time prolonged to intersect the horizontal axis whose origin was shown by a small circle, and the ab-scissa of the intersecting point was examined, from which it could positively be said that the points of intersection gathered near the origin.

A similar tendency could also be found in other conditions of impact, which demonstrate that the test results on the drop height can be said to coincide approximately with the theoretical prediction on the present problem under discussion.

The drop height is generally kept costant in almost every kind of apparatus for dynamic penetration tests, and so this subject of investigation has no direct effect on this method of sounding. But it may contribute to the theoretical

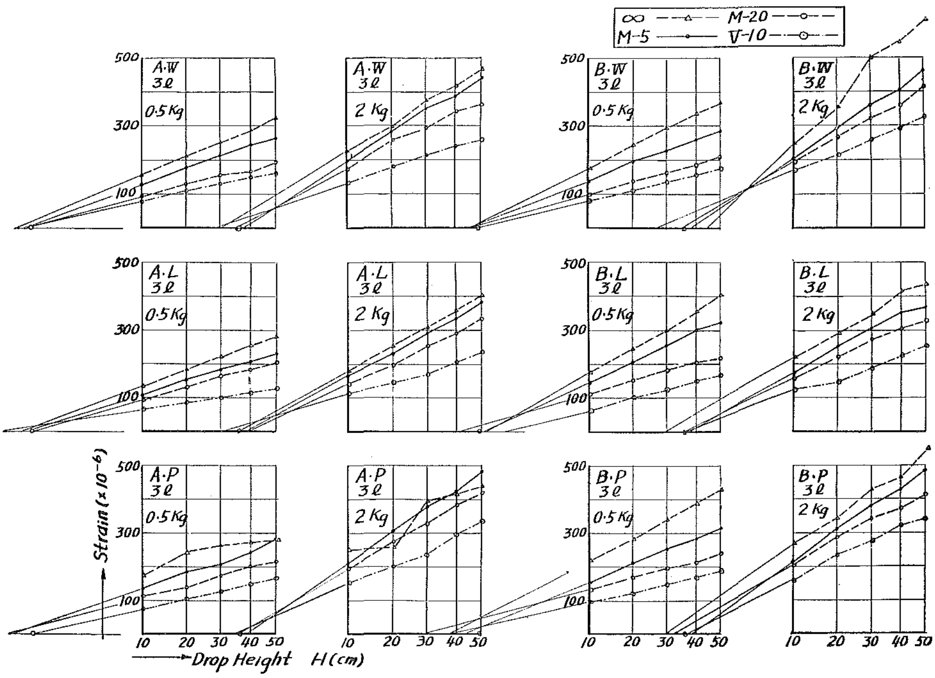

Fig. 13. Strain-$\sqrt{H}$ curves ($3l$)

improvement of the dynamic pile driving formulas, especially when the efficiency of impact due to the drop height comes into question.

(2) **Effect of rod length**

A penetration index N, which is the number of blows per certain depth of penetration, should be reduced for larger lengths of the penetration rod, compared to shorter ones, when it penetrates into a foundation soil with the same resistance to penetration under the same conditions of driving 8), 9), 10).

Under the constant weight of rammer, the weight ratio m decreases in value when the length of the rod is lengthened, for example m becomes 2.5 if the length of the rod, whose weight is one fifth of the rammer, is made twice as long. The value of q is not changed by the length of rod as shown before; it follows that the difference between the ordinate of the $m=5$ curve and the $m=2.5$ curve for a certain value of q in Fig. 5 is the theoretical decrease of the created strain at the end of the rod due to the elongation of the rod by 2 times, the weight of rammer and the strength of k-body being constant. Thus the full lines in Fig. 14 were obtained to show these theoretical decreases of strain due to increase of the length of the rod for various values

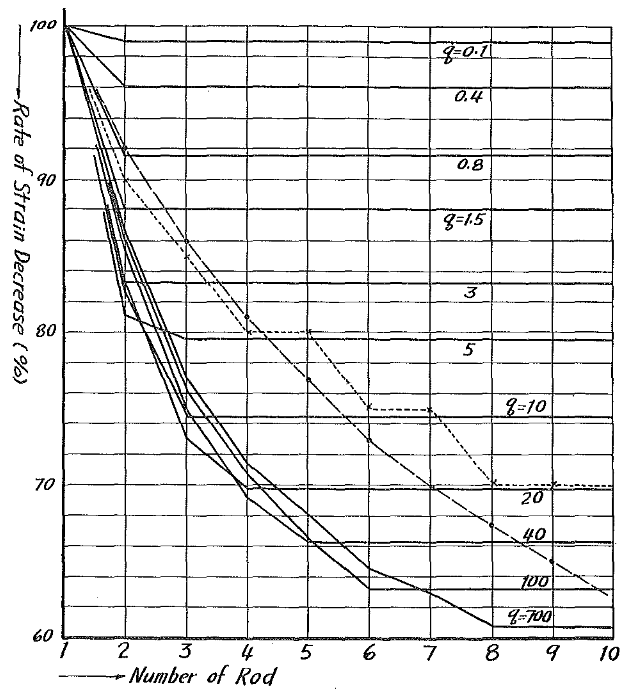

Fig. 14. Theoretical rate of strain decrease at rod end due to increase of rod length.

of q, making the case for $m=5$ the standard of comparison. The weight ratio of $m=5$ corresponds approximately to the Standard Penetration Test by Terzaghi and Peck with the 3 metres length of the sounding rod. The dotted or broken lines in Fig. 14 are the coefficients to be applied in reducing the N value according to the length of the rod, given in the reference 8), 9). Some similarity can be seen among these three kinds of curves, although the curves in the above references were not always based on theoretical investigation.

If N is assumed to be proportional to the created strain at the end of the rod, it can be said from Fig. 14 that:

1) the rate of decrease in the created strain due to the increase of the rod length differs according to the value of N. This means that the reduction of N should be determined by N itself, together with the length of the rod, because N is assumed to the proportional to the strain and the strain was shown to be a function of q in Fig. 5.

2) the rate of decrease becomes constant, when the length of the rod exceeds a certain limit, which means that the coefficient of reduction is unchanged in

such a condition. But this theoretical conclusion may be considered to be opposed to the actual circumstances, and it must be examined by laboratory experiments.

3) the rate of decrease becomes small as q decreases, which shows that the reduction of N should be small when the penetrated soil layer is not firm, even when the rod is very long.

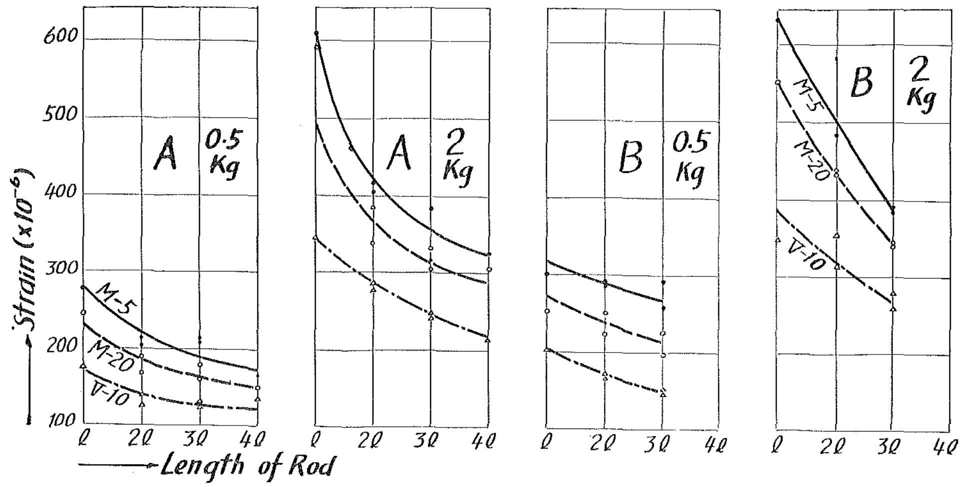

Fig. 15. Decrease of observed strain at rod end due to increase of rod length (P-Series, H=30 cm).

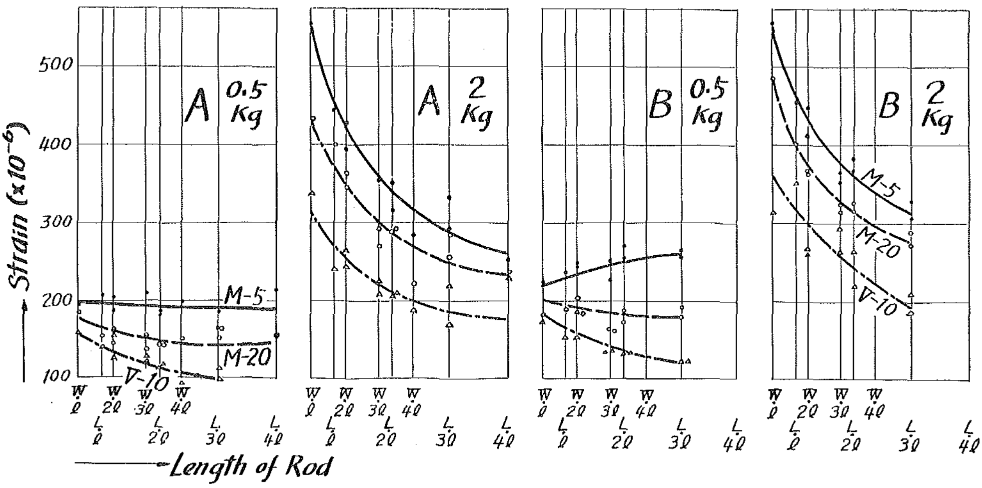

Fig. 16. Decrease of observed strain at rod end due to increase of rod length (L, W-Series, H=30 cm).

These theoretical conclusions concerning the effect on the strain created at the end of the rod due to increase of the rod length were examined in accordance with the results of the experiment. As mentioned before, there were four categories of length of rod for each rod series in this experiment and efforts were concentrated on the measurement of strain at the ends of the rods. The test rods of the L-Series have the same characteristics with those of the W-Series in their material and cross section and so forth, except for their length. Then it could be possible to plot the test results of both series together and to divide the rod length of the L-Series by the unit length of the W-Series, by which the rod length of the L-Series could temporarily be considered to be $6l$ in spite of its real number of $4l$, whereas the division of the rod length would remain $4l$ for the P-Series.

Fig 15 and 16 are two examples out of the plottings done in this manner and the curves were drawn free hand. Except for k-body M-5 in the B-Test, the strain seemed to decrease regularly according to the rod length. Based on

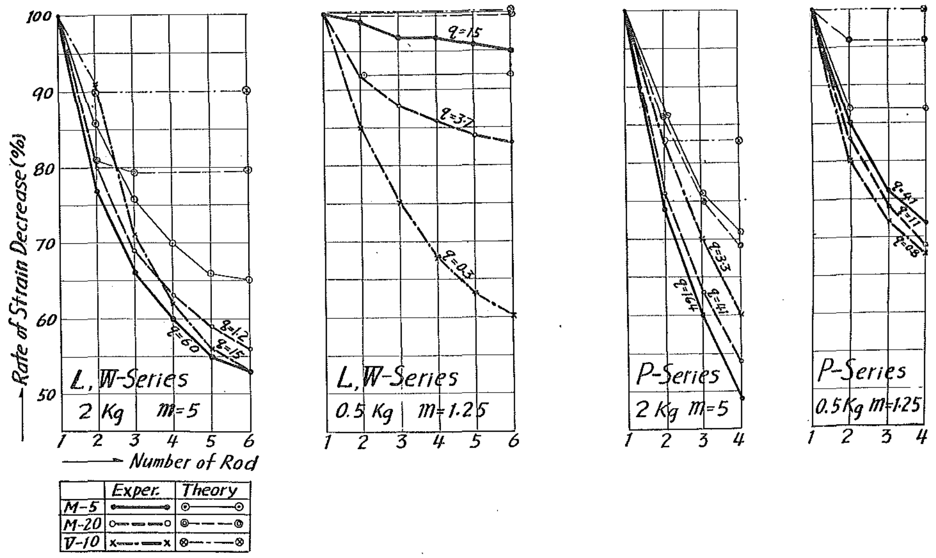

Fig. 17. Experimental rate of strain decrease at rod end due to increase of rod length (H=30 cm).

these curves, rates of decrease are shown in Fig. 17, in which the thin curve lines show the theoretical rate of decrease for corresponding values of q. From these curves, it may be concluded that:

1) theoretical conclusions concerning the rate of decrease due to the increase of the rod length were also found to be almost correct by the experiment.

2) the rate of decrease did not cease to increase for each value of q as indicated by the theory, but continued to increase in the experiment. This might show the existence of other kinds of losses of impact which were not involved in the fundamental equations of strain.
3) the rate of decrease obtained from the results of the experiments was larger than that from the theory.

The actual coefficient of reduction due to the increase of the rod length should be determined either by laboratory experiments using soil samples in place of elastic k-dodies or by statistic treatments of the test results taken in the field. On such an occasion, the present theoretical and experimental conclusions on this subject can serve as a fundamental concept for determining the coefficients.

(3) Rammer weight

It can be shown that the soil resistance at the end of a pile is proportional to the rammer weight in accordance with the simple formula for dynamic pile driving by Sander. Discussions were made hereafter as to whether the strain at the end of the rod increases in proportion to rammer weight or not.

In this experiment, 4 rammers were used as mentioned before. Fig. 18, 19 and 20 show the increase of strain due to the increase of the rammer weight for several conditions of impact in the A-Test. Fig. 21 shows the ratio of the increased strain to the strain of $G=0.25$ kg, which indicates that the

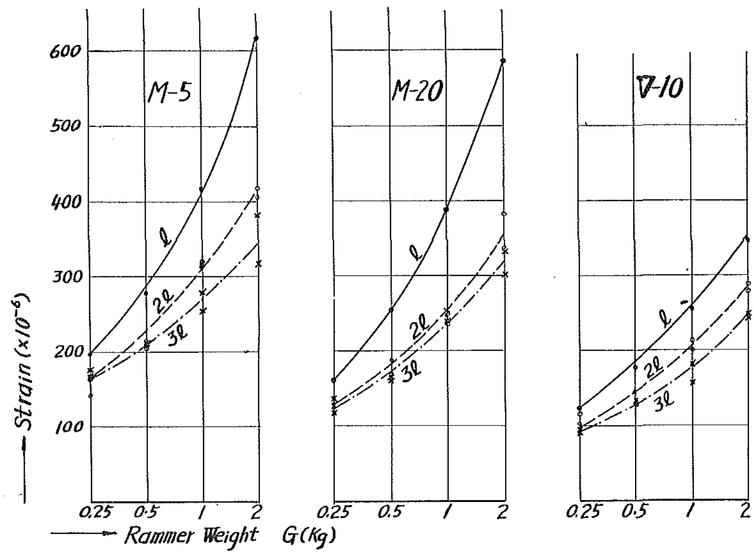

Fig. 18. Rammer weight and strain (P-Series, $H=30$ cm).

ratio increases as the length of rod becomes shorter and also the rammer weights heavier, and that it seems to be independent of the drop height.

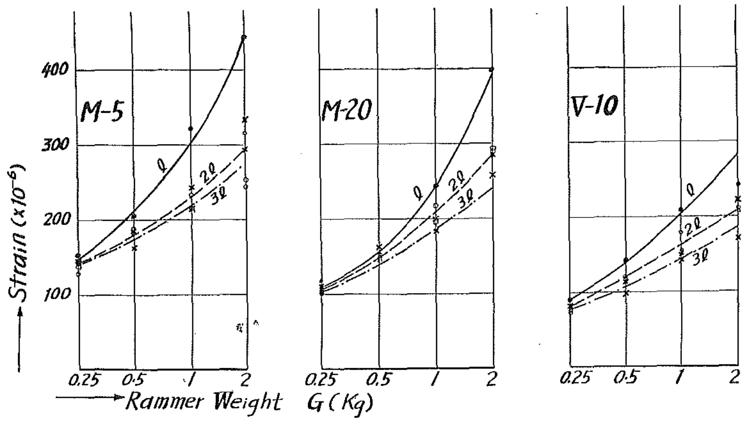

Fig. 19. Rammer weight and strain (L-Series, $H=30$ cm)

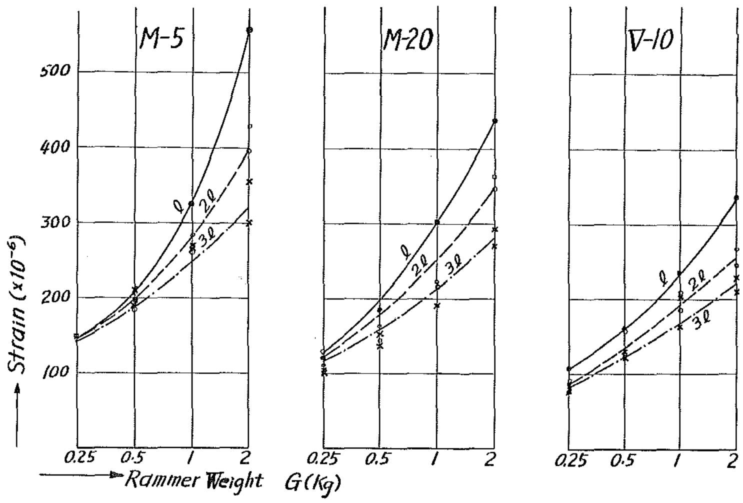

Fig. 20. Rammer weight and strain (W-Series, $H=30$ cm).

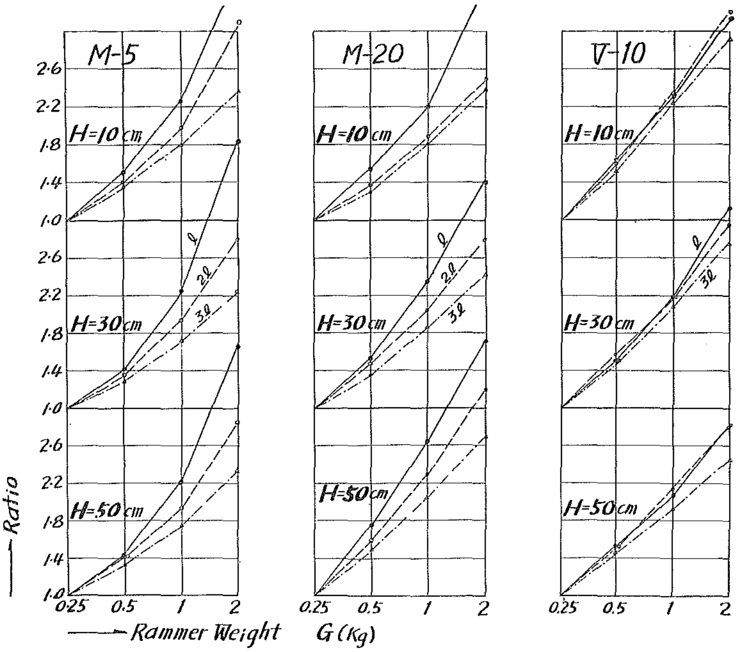

Fig. 21. Experimental ratio of strain increase at rod end due to increase of rammer weight (W-Series).

The theoretical increment of strain due to the increase of the rammer weight can easily be calculated from Fig. 5, keeping the rod length constant and changing weight of rammer from 0.25 kg to 2 kg. Similar ratios based on these theoretical values were also calculated in the same manner as in the forgoing case, and the following ratios were obtained, one of which is shown in Fig. 22.

$$\frac{\text{(ratio of strain increase by experiment)}}{\text{(ratio of strain increase by theory)}}$$

From this figure and others which are not shown here, it can be seen that the ratio of increment was larger by experiment than by theory.

The experimental results indicated that the strain at the end of the rod for the length l by the 2 kg rammer was approximately 3 times as much as that by the 0.25 kg rammer, which showed that the strain at the end of the rod rose only 3 times in spite of an increase of rammer weight by 8 times. Therefore, the soil resistance at the end of piles might not be proportional to the rammer weight as deduced from Sander's or other similar types of dynamic pile driving formulas. The condition of the pile end comes near to an elastic state in the

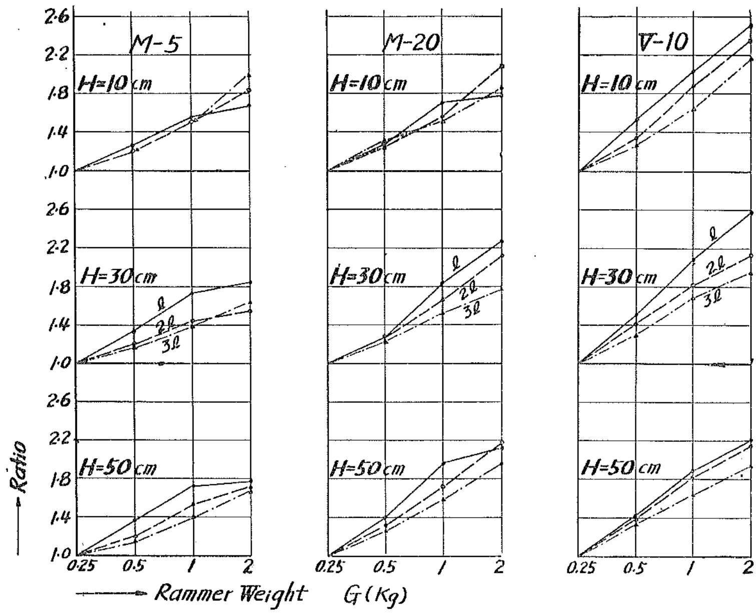

Fig. 22. $\frac{\text{(experimental ratio of strain increase)}}{\text{(theoretical ratio of strain increase)}}$ (L-Series)

last stage of driving, which may agree approximately with the assumed boundary condition of the fundamental equations in the present investigation.

(4) **Effect of Joints**

The transmission of impact stress to the end of the rod may be interrupted by the existence of joints, even when the jointed rod is completely straight, because screw joints make points of discontinuity in rods which may produce certain amounts of energy losses, and the rods cannot act like continuous material of an elastic body. It may naturally be assumed that there will be some loss of energy in longitudinal impact, if the rod should happen to vibrate transversely for lack of straightness caused by the joints. It is very difficult to deal theoretically with this problem, and this subject can only be examined by the results of the expeiments.

Fig. 23 and 24 show some of the following values

$$\frac{C-D}{C} \times 100 ,$$

in wich C is strain at rod end for jointless rods and D is for jointed rods, in the same series with equal length and weight. If a disturbance of strain transmission as a result of joints occurs, the value is to be positive, but it does not

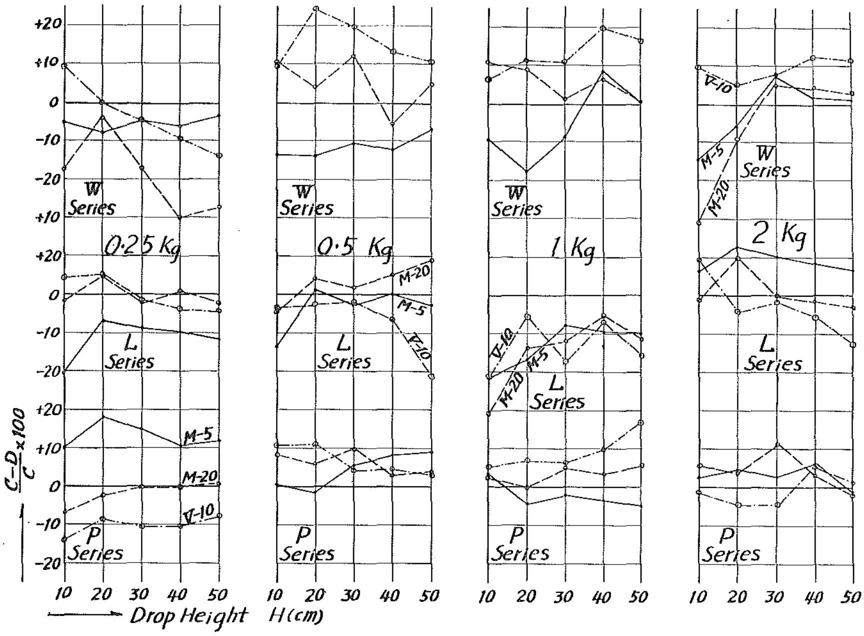

Fig. 23. Effect of joints (A-Test, $2l$ and $2\times l$).

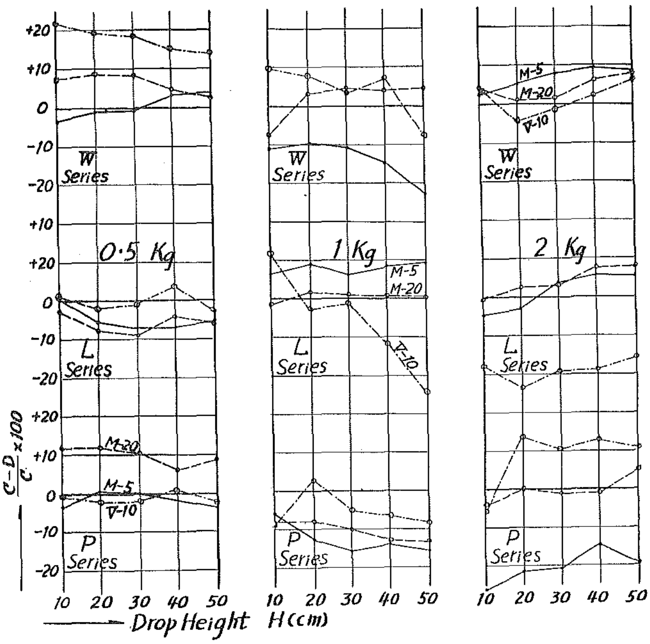

Fig. 24. Effect of joints (B-Test, $2l$ and $2\times l$).

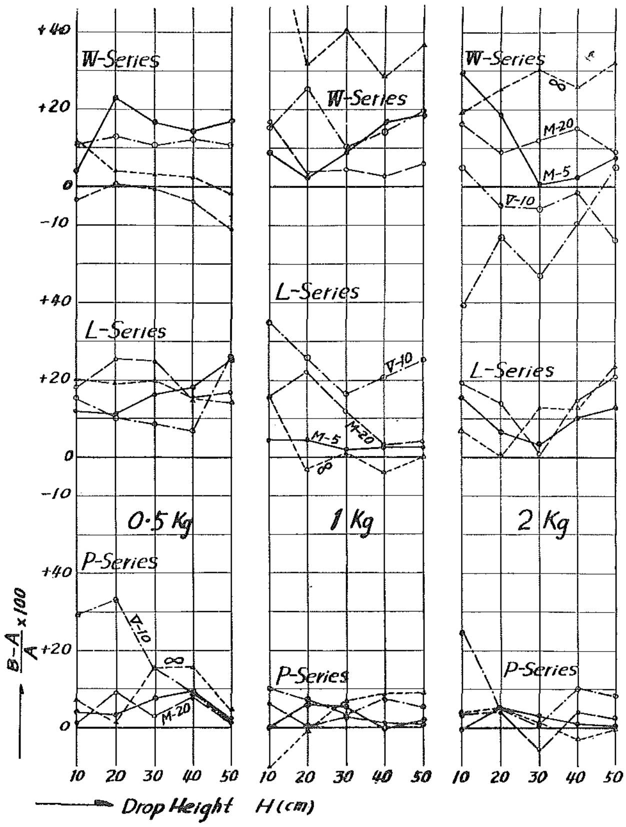

Fig. 25. Comparison of A-Test with B-Test (l).

seem to be always positive, judging from the above figures and other data on this subject.

There are two other data for the discussion of this problem, one of which is the comparison of exerted strains in both gages set above and below the joint as shown in Fig. 11. For example, strains measured by gage No. 6 and 7 in a rod of $2\times l$ for each series may be larger than those by No. 4 and 5, if the joint should interrupt transmission of the strain. The other was the comparison of the mean values for intermediate points both of jointed rods and jointless ones with equal length for each series. For example, if an interruption should occur, the average of No. 4 and 5 gages in a rod of $2l$ without a joint would be larger than that of No. 4, 5, 6 and 7 in a rod of $2\times l$ with a joint for each series. But, contrary to the author's expectation, the two comparisons showed that the one was not always larger than the other.

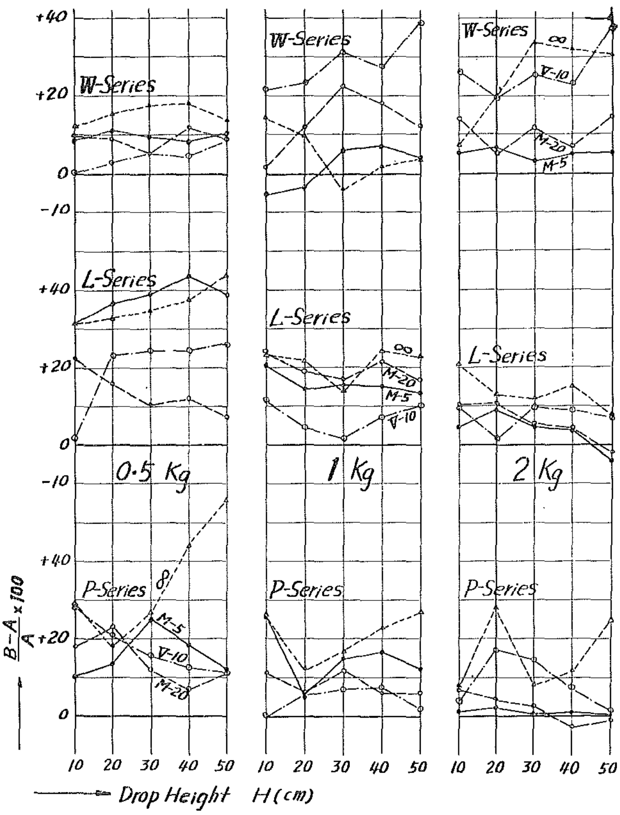

Fig. 26. Comparison of A-Test with B-Test ($3l$).

In this experiment, a great deal of care was taken to make the test rod to stand exactly vertical and to screw the joint as tightly as possible. From this fact and the above mentioned results of the experiments, it might be concluded that the transmission of impact stress through penetration rods was hardly interfered by the existence of joints, as long as the rod was precisely straight and its joint was screwed tightly.

(5) Comparison of A-Test with B-Test

The experimental results of the B-Test should be larger than those of the A-Test, the reason for this has already been explained.

In Fig. 25 and 26, some of the values of (B-A)/A are shown in percentages, in which A and B are the results in the two corresponding experiments. These figures indicate that the test results of the B-Test are almost always larger than those of the A-Test by aproximately 16 %. This might also indicate the correctness of the assumed boundary condition at the end of the rod, and at the same time the fundamental equations which give the strains at this point.

(6) **On the type of rod**

It is discussed here how much force was exerted at the end of the rod in each kind of series under the same condition of impact. Based on this discussion, the author intended to examine, what type of rod was most suitable as a penetration rod, the solid round bar of the L-Series with equal length to the P-Series, or that of the W-Series with equal weight to the P-Series. The ratio S_l and S_w of total forces in the Series of L and W, divided by those in the P-Series with the same designation and condition of impact to each other, were calculated as follows.

$$S_l = \frac{A_l}{A_p} \cdot \frac{\varepsilon_l}{\varepsilon_p} \quad \text{and} \quad S_w = \frac{A_w}{A_p} \cdot \frac{\varepsilon_w}{\varepsilon_p},$$

where the suffixes p, l and w are for the series of P, L and W. A and ε are the sectional area and the strain exerted at the end of the rod. In this experiment, the ratio of the sectional area, A_l/A_p and A_w/A_p were both 1.71. Table 13 shows the values of S_l and S_w which were theoretically calculated. The L-Series, from this Table, gave forces larger than the P-Series by 20 to 60% and the W-Series by 40 to 60%.

TABLE 13. Theoretical Values of S_l and S_w

k-body	S_l / S_w	Rammer weight							
		0.5 kg				2 kg			
		Length of rod				Length of rod			
		l	$2l$	$3l$	$4l$	l	$2l$	$3l$	$4l$
M- 5	S_l	1.53	1.59	1.59	1.59	1.44	1.36	1.36	1.43
	S_w	1.53	1.59	1.59	1.59	1.60	1.58	1.57	1.55
M-20	S_l	1.51	1.51	1.51	1.51	1.29	1.22	1.38	1.53
	S_w	1.51	1.51	1.51	1.51	1.46	1.42	1.40	1.53
V-10	S_l	1.55	1.55	1.55	1.55	1.26	1.48	1.48	1.48
	S_w	1.55	1.55	1.55	1.55	1.36	1.48	1.48	1.48

Fig. 27 shows the ratios of S_l and S_w which were calculated from the results of the experiments. The values of S_l and S_w seemed to vary between 1.2 and 1.8, which meant that the L and W-Series could create forces 20 to

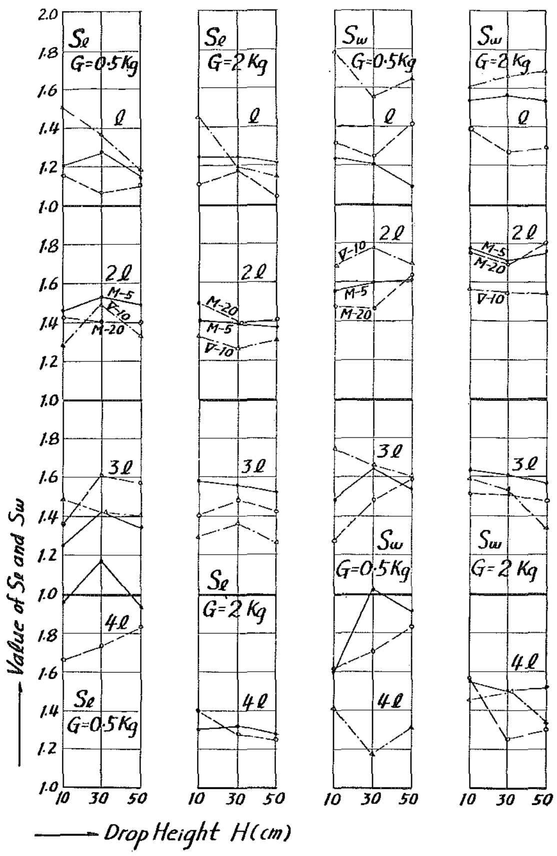

Fig. 27. Values of S_l and S_w by experiment.

80% larger than the P-Series. The ratio of the theoreticol S_l and the experimental S_l was found to be almost in unity and this was the same in the case of S_w, which showed close agreement of the experiment with the theory.

The rods of the L-Series, as stated before, have equal length to those of the P-Series, and created forces 20 to 80% larger than the P-Series, but their weights were larger by 70% than those of the P-Series. Then it could be said that penetration rods of solid bar compared with tubular rods of equal length can not create forces proportional to their greater weights. On the other hand, the W-Series with rods of equal weight to the P-Series created greater forces, but their lengths were about 60% of those of the P-Series, which was considered to be inconvenient for field work.

From the above discussions, it was concluded that a penetration rod of steel pipe was suitable for its transmission of impact force, from the standpoint of length and weight of rod.

(7) **On the value of q**

q is a very important number in the present investigation. This can be seen, for example, in plotting the strain-m, q curves, which are a basis of this study and are discussed in the next paragraph.

Under the assumption of $E'=n_1E$ and $A'=n_2A$, q will be transformed as follows;

$$q=\frac{G}{\gamma A}\cdot\frac{n_1n_2}{l'},$$

and $n_1=1$ for metalic k-bodies and $n_2=1$ for the L and W-Series. G, A, γ and l' should remain unchanged during the impact, but a question arose, as to whether the *statically* determined E and E' should change their values as a result of the *dynamic* application of impact loads. It is discussed here-after as to whether the values of q in Table 3 to 5 calculated from the statically determined E and E' are correct or not.

Fig. 28 is a strain curve for a certain value of m, in which X is a theoretical strain for $q=\infty$ and x is its experimental one; Y is a theoretical strain for a certain value of q and y is its experimental one. The ratio of strain decrease from X to x may be equal to that of Y to y, because there is no difference between these two cases, except for the existence of k-bodies.

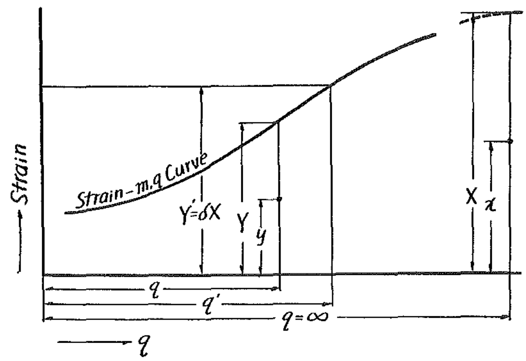

Fig. 28. Relation between q and q'.

Then

$$\frac{x}{X}=\frac{y}{Y},\quad Y=\frac{y}{x}X=\delta X$$

When m is less than 5.6, X is easily calculated as follows 11).

$$X=-2\frac{V}{a}(1+e^{-2/m})$$

Therefore, if δ can be acquired, then Y can also be determined. When the values of strain for infinity in Table 7, 8, 10 and 12 were used as the values of y, semi-experimental values of Y' can be calculated. The ab-scissa q', corresponding to the ordinate Y' is acquired as shown in Fig. 28. If $q=q'$, the statically determined q can be considered sufficiently correct for this investigation.

Fig. 29. is an example of q'/q to examine the coincidence of q and q', and it was evident that the deviation from unity of the values of q'/q was not small. There were some cases in which Y' was too large to plot the value of q'/q, which showed that the observed values for infinity were too small.

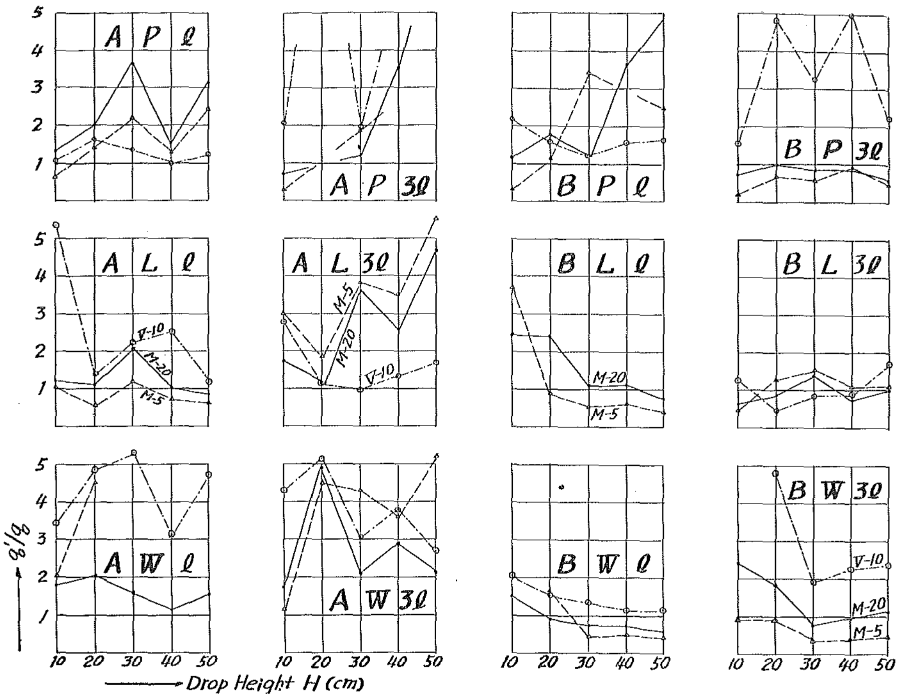

Fig. 29. Values of q'/q ($G=2$ kg).

Fig. 29 seems to show that the values of q'/q which are larger than unity, hold an overwhelming majority, and so q' does not coincide with q. But q' may on the whole be equal to q for the following two reasons, one of which is that the number of values for q'/q, which lie between 0 and 2, amounts to 333 out of 630, so that half of them are close to 1. The other is that the values of q'/q, which lie between 0 and 2, can be observed to concentrate around 1.

Therefore q' can be said to be nearly equal to q, and the Young's modulus for both the rod and the k-body by static definition can be concluded to be sufficient for dynamic penetration problems, as far as the results of the present experiments are concerned. In the next paragraph, statically calculated values of q were used in plotting the strain-m, q curves.

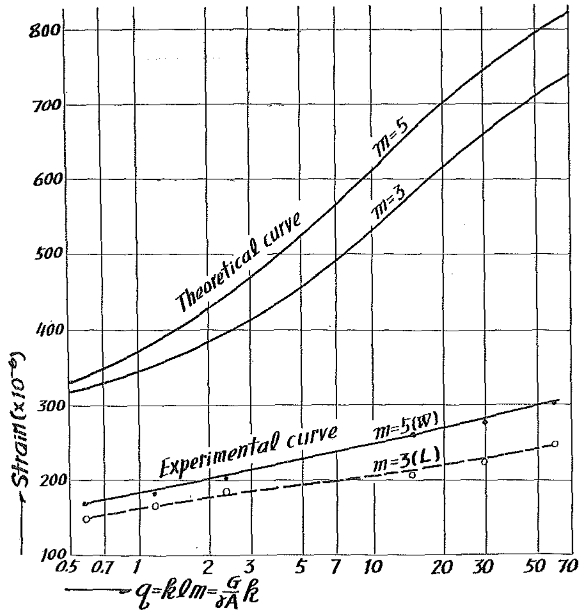

Fig. 30. Strain-m, q curves (L, W-Series, H=10 cm, m=5, 3)

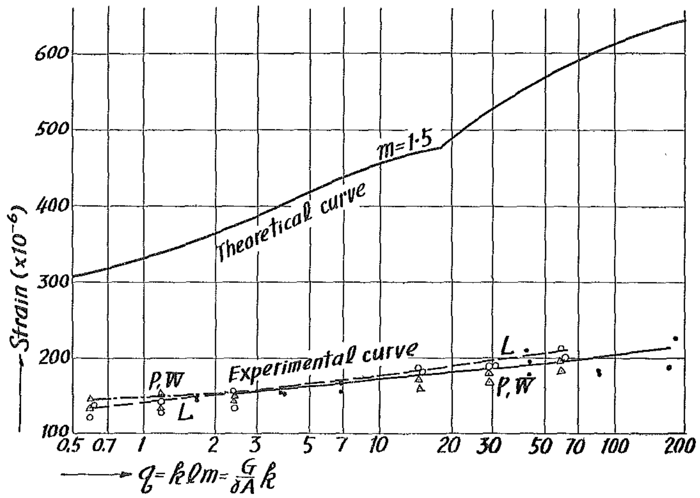

Fig. 31. Strain-m, q curves (P, L, W-Series, H=10 cm, m=1.5).

(8) **Strain-m, q curves**

Strain-m, q curves in Fig. 5 are one of the most important results in this investigation and it is discussed here-after whether these theoretical curves agree with the experimental results.

Fig. 30, 31, 32 and 33 show some of the test results in which rammer weight G and weight ratios m were used as a basis for plotting the curves.

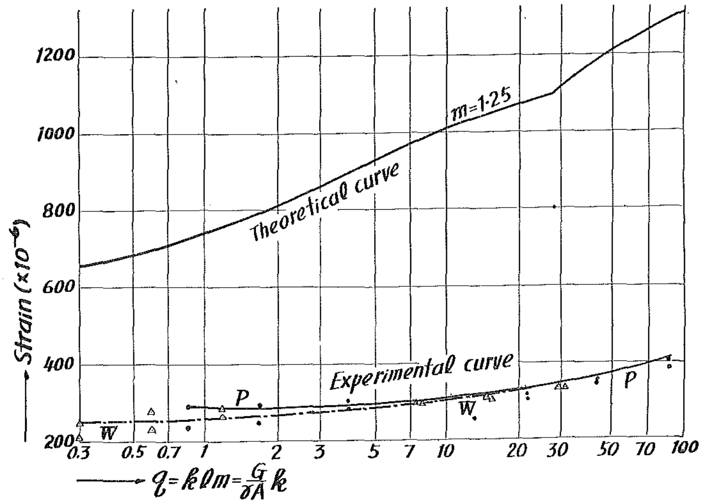

Fig. 32. Strain-m, q curves (P, W-Series, H=50 cm, m=1.25).

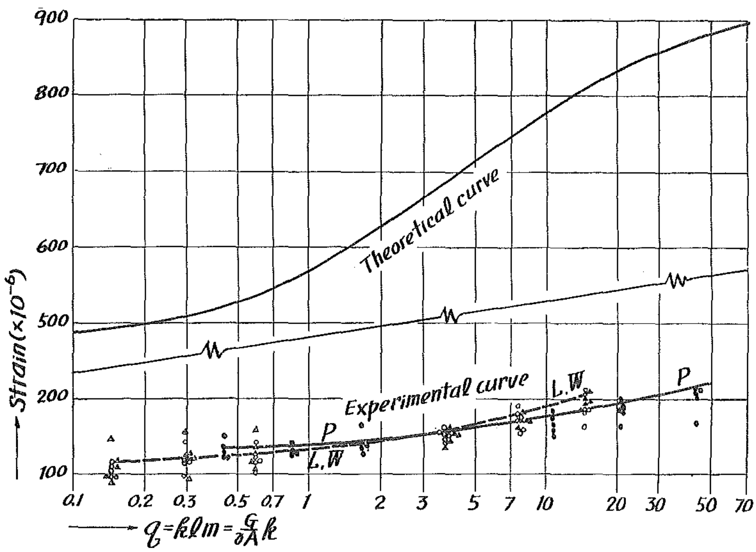

Fig. 33. Strain-m, q curves (P, L, W-Series, H=30 cm, m=0).

Strain curves for experimental results were drawn so as to pass through the upper parts of the plotted strains, which scattered to some extent on a vertical line for any given value of q. The reason for this manner of drawing the curves was that the experimental decrease of the strain at the end of the rod due to the increase of the rod length was larger than the decrease calculated theoretically, and then if the test results for the shortest rods were taken as standard, a strain-m, q curve for the experimental results should pass through the upper part of the scattered observed strains.

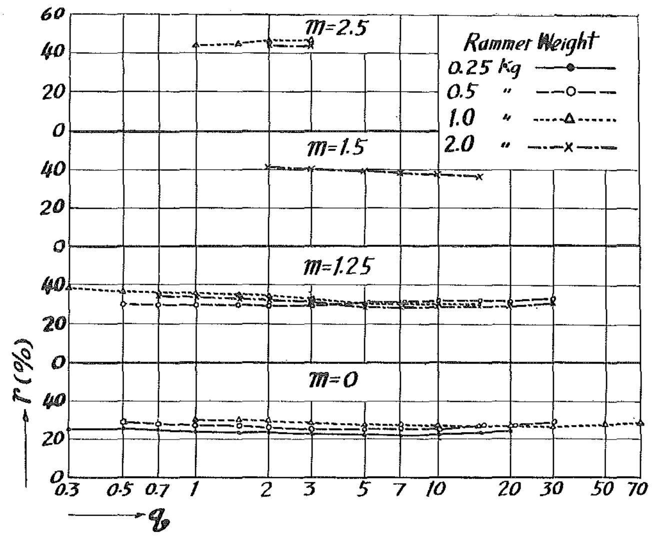

Fig. 34. Values of r (P-Series, H=10 cm).

In Fig. 34 the values of r, when

$$r = \frac{\text{(experimental strains)}}{\text{(theoretical strains)}},$$

for each value of q are shown in percentages in order to examine the similarity of the experimental strain curves to the theoretical ones. Both curves can be said to be similar if r has approximately equal values for all values of q. Fig. 34 indicates that the curves of r are nearly horizontal for almost every condition of impact, and the values of r are nearly indendent of q. The differences between the maximum and minimum values of r in a certain strain curve by experiment are shown in Table 14 and 15, in which the value of this difference has plus sign when the maximum value of r can be found on the left hand side of the curve and a minus sign when on the right.

TABLE 14. Discrepancies in the Values of r for a Given Value of m
(first period, in %)

m	Rammer weight (kg)	H=10 cm P	H=10 cm L	H=10 cm W	H=30 cm P	H=30 cm L	H=30 cm W	H=50 cm P	H=50 cm L	H=50 cm W
2.5	2	1		2	1		1	3		−3
	1	−2		6	−1		1	−6		7
1.5	2	4	3	8	3	3	2	5	5	3
	1		−2			10			2	
1.25	2	5		5	2		6	1		2
	1	8		11	9		12	10		9
	0.5	−3		4	−3		8	−5		4
1	2		−6			3			−2	
0	2		−1			0			0	
	1	3	4	6	−6	3	−2	−5	3	−3
	0.5	2	−2	−2	2	−3	−3	4	−2	2
	0.25	4	−1	−1	2	−4	−4	0	−3	−3

TABLE 15. Discrepancies in the Value of r for a Given Value of m
(second period, in %)

m	Rammer weight (kg)	H=10 cm P	H=10 cm L	H=10 cm W	H=30 cm P	H=30 cm L	H=30 cm W	H=50 cm P	H=50 cm L	H=50 cm W
5	2	5		12	−3		15	−3		14
3	2		13			6			5	
2.5	2	8		9	8		7	8		7
	1	9		6	9		11	8		10
1.5	2	4	3	4	2	2	2	1	2	2
	1		0			1			0	
1.25	2	−1		−1	3		−1	2		0
	1	0			1			1		
	0.5	0			1			0		

The absolute values of these differences varied from 0 to 15% and those with plus signs amounted to 81 examples out of 122. Thus it may be concluded that both curves were almost completely similar, although there was, as a whole, a tendency for the experimental curves to have smaller ordinates than the theoretical ones for the larger values of q.

Next, the absolute values of r will be discussed. From this, it is possible to examine the extent of loss of impact, and how they were affected by the length of rod and rammer weitght, together with some other factors left unchecked.

Table 16 and 17 show the mean values of r, in which the designation of $m=0$ means that every combination of m and q which falls into this category, belongs to the first period of elastic vibration, in which the maximum strain occurs in that period as already explained in part I.

TABLE 16. Mean Value of r, Arranged Mainly According to Values of m (in %)

m	Rammer (kg)	$H=10$ cm				$H=30$ cm				$H=50$ cm				Total Mean
		P	L	W	Mean	P	L	W	Mean	P	L	W	Mean	
5	2	41		44	43	42		44	43	40		44	42	43
3	2		37		37		37		37		38		38	37
2.5	2	45		47	46	42		46	44	41		46	44	45
	1	46		44	45	43		44	44	43		43	43	44
	Mean	46		46		43		45		42		44		
1.5	2	39	41	41	40	37	37	38	37	37	36	35	36	38
	1		35		35		34		34		36		36	35
	Mean	39	38	41		37	36	38		37	36	35		
1.25	2	32		32	32	32		30	31	33		29	31	31
	1	34		32	33	30		33	32	33		33	33	33
	0.5	31		30	31	32		29	31	33		31	32	31
	Mean	34		31		31		31		33		31		
1	2		35		35		36		36		34		34	35
0	2		27		27		28		28		27		27	27
	1	28	31	34	31	31	29	31	30	30	28	30	29	30
	0.5	27	27	27	27	24	24	24	24	24	24	25	24	25
	0.25	24	21	21	22	23	20	20	21	21	20	19	20	21
	Mean	26	27	27		26	25	25		25	25	25		

TABLE 17. Mean Value of r, Arranged Mainly According to Rammer Weight (in %)

Rammer (kg)	m	H=10 cm				H=30 cm				H=50 cm				Total Mean
		P	L	W	Mean	P	L	W	Mean	P	L	W	Mean	
2	5	41		44	43	42		44	43	40		44	42	43
	3		37		37		37		37		38		38	37
	2.5	45		47	46	42		46	44	41		46	44	45
	1.5	39	41	41	40	37	37	38	37	37	36	35	36	38
	1.25	32		32	32	32		30	31	33		29	31	31
	1		35		35		36		36		34		34	35
	0		27		27		28		28		27		27	27
	Mean	39	35	41		38	35	40		38	34	39		
1	2.5	46		44	45	43		44	44	43		43	43	44
	1.5		35		35		34		34		36		36	35
	1.25	34		32	33	30		33	32	33		33	33	33
	0	28	31	34	31	31	29	31	30	30	28	30	29	30
	Mean	36	33	37		35	32	38		35	32	35		
0.5	1.25	31		30	31	32		29	31	33		31	32	31
	0	27	27	27	27	24	24	24	24	24	24	25	24	25
	Mean	29	27	29		28	24	27		29	24	28		
0.25	0	24	21	21	22	23	20	20	21	21	20	19	20	21

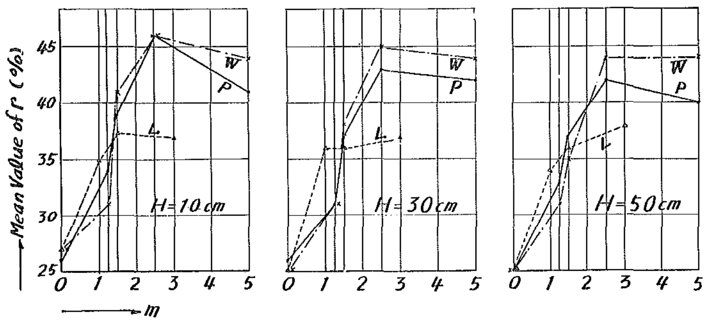

Fig. 35. Relation between m and mean value of r.

The values of r varied from 20 to 50%, and the loss of impact, considering every condition of impact, reached as much as 50 to 80%. Fig. 35 illustrates the relation between m and the mean value of r, and the details of strain-m, q curves will be discussed on the basis of this figure and the above mentioned Tables.

r and drop height

All the data on r seemed to show that it had almost nothing to do with the drop heights of the rammers and this conclusion can easily be predicted from the linear relationship between the strains and the square roots of the drop heights, which has already been demonstrated in the above section.

r and series of rods

The rods of the P and W-Series had equal weights to each other for certain designations of rod, and their values of m were equal for a certain rammer weight. Then the test results of both series with the same value of m, should make a single curve for various values of q, and Table 16 and Fig. 35 demonstrate that this theoretical prediction was also correct for the results of the experiment.

These two series have been discussed up till now as if they belonged to different categories, since it was supposed that the difference in the cross section of the test rods for both series might give an unexpected experimental effect on the strain at the end of the rod, notwithstanding their identity to each other from the theoretical point of view, but now it has become unnecessary to distinguish the test results of the W-Series from those of the P-Series.

According to the theory, this conclusion should also be expanded to the series of L which had rods of equal length with those of the P-Series, but had different weights and values of m. This means that the experimental curves of r for the L-Series should coincide with those for the P and W-Series, at least in the first period. In this period of vibration the values of r for the L-Series can be seen, in Fig. 35, to separate considerably from those of the P and W-Series, but their amount of difference reached only 5%, and then the L-Series can also fall into the same category with the other two series as it may be concluded from the present theory.

It has been clear from the above discussions on the experimental results that, insofar as the values of m were equal, there was no need to make any distinctions between these three types of rods by their length, weight and cross section, as it can easily be seen from the fundamental equations on the maximum strain at the end of the rod. This can be considered to be one of the experimental verifications of the present fundamental equations.

r and m

Table 16 ane Fig. 35 show that the values of r are nearly equal to each other for a certain value of m, independent of drop height, the types of rod and so forth, but for another value of m, the values of r are somewhat different from the forgoing one. Fig. 35 also shows that r seems to be approximately proportional to m when it is less than 3. The smaller values of m correspond to lightly weighted rammers or longer lengths of rod. Then it can naturally be considered that there might occur an excess decrease of strain at the end of the rod due to the increase of the rod length in the experiment, as compared with that of the theory. The values of r would be equal for all values of m, if the experimental decrease of strain due to the increase of the rod length should happen to have equal ratios to the theoretical decrease for every value of m, but the decreases in the experiment were larger in the case of smaller values of m than in the case of larger values of m, as previously demonstrated in Fig. 17. For the larger values of m of 3 to 5, in Fig. 17, the rate of strain decrease in the experiment can be considered to be close to that reached by the theory. From this experimental fact, r remains nearly constant in Fig. 35 when m is more than 3, in which case the maximum strain occurs in the second or the third period of vibration, and it can easily be concluded that the reason why r was approximately proportional to m should be attributed to the strain decrease due to the increase of the rod length.

Against this conclusion, the values of r for $m=0$ were different from each other, but this fact was also attributed to the strain decrease due to the increases of the rod length as follows. In the category of $m=0$, which was merely determined for convenience, there was a range of m from 0.1 to 0.8, and therefore there should naturally occur an excess decrease of strain in the case of the experiments, at the rod ends due to the increase of the rod length, and so there were some differences in the values of r, even when $m=0$.

Strain curves and rammer weight

It is discussed herein-after as to whether the strain-m, q curves have their own peculiar configuration in accordance with the magnitude of the rammer weights.

In the fundamental equations of the strains at the rod end, (8), (9), (10) and (11), the strains are the functions of m and q when the drop height of rammer and the mechanical proporties of rod are fixed. Then it follows that the strains exerted at the end of the rod should always coincide with each other, regardless of the make-up of q, $(k \times l \times m)$, insofar as the absolute values of m and q are equal respectively, if no loss is sustained during impact. On the other hand, however, it may well be considered that the strain-m, q curves obtained by using two different weights of rammers, should have their own peculiar configurations, because the make-up of q, ($kG/\gamma A$, see Part I) is different for these two cases of the two rammer weights even when the two values of q and the two values of m are respectively equal, suitable values of k being given, and also there can be, in these two cases, any other combinations of $G/\gamma A$ and k for rendering the two values of q equal to each other, keeping the value of m always constant.

In Table 18, all the cases in which each group of the experiments has the same value of m and also the same value of q respectively, are gathered together, regardless of series, k-bodies, rammer weights and rod lengths in order to examine whether the strain-m, q curves should be distinguished at least by the rammer weight. The ratios of strains for any value of q to those for the corresponding values of q in the tests of the P-Series with the rammer weight of 2 kg are given in this table, which demonstrates that the test results for the strain-m, q curves need not be distinguished by rammer weight.

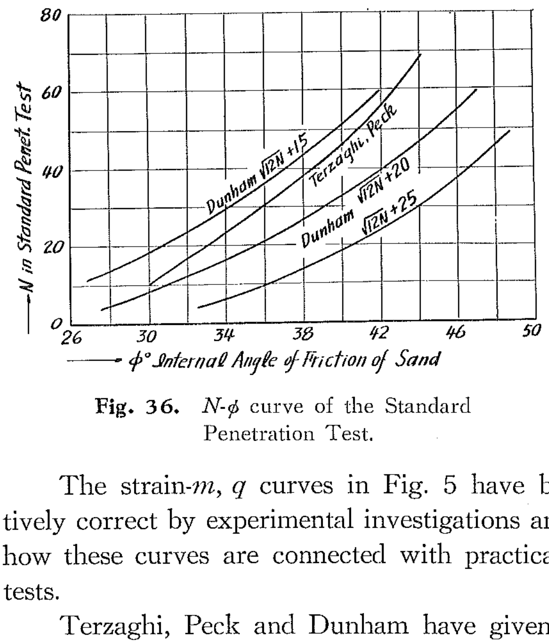

Fig. 36. N-ϕ curve of the Standard Penetration Test.

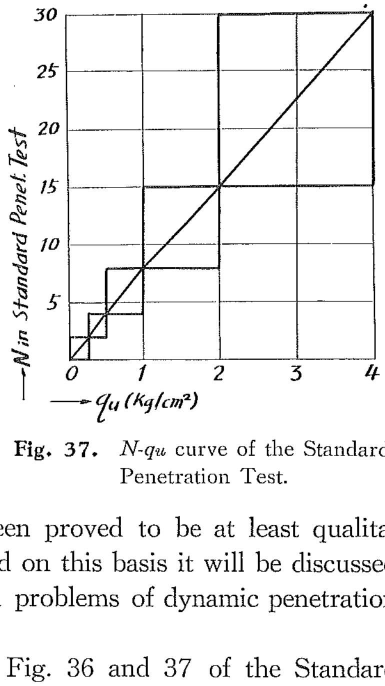

Fig. 37. N-q_u curve of the Standard Penetration Test.

The strain-m, q curves in Fig. 5 have been proved to be at least qualitatively correct by experimental investigations and on this basis it will be discussed how these curves are connected with practical problems of dynamic penetration tests.

Terzaghi, Peck and Dunham have given Fig. 36 and 37 of the Standard Penetration Test to show the relation between the number of blows per certain depth (penetration index, N) and the internal angle of friction (ϕ) or unconfined compressive strength (q_u) of soil. Now the transitional part of the strain curve from the first period to the second for $m=2.5$ in Fig. 5 was compared against the well-known Terzaghi and Peck's curve in Fig. 36, and both curves were found to coincide with each other to a considerable degree. This could be said to be the same with Dunham's curves. The strain curves for smaller values

TABLE 18. Ratios of Strain for Cases where the Values of m and q are equal

Drop height (cm)	Standard Series Rammer	Standard m	Series	Rammer (kg)	Value of q: 2	3	5	7	10	15	20	30	50	70	100	150
10	P, 2 kg	2.5	P	1	1.05	1.07	1.03	1.03	1.03	1.03	1.03	1.01	1.00	0.97		
			W	2	1.07	1.06	1.16	1.18	1.20	1.22	1.22	1.22	1.19	1.15		
			W	1	0.94	0.94	0.93	0.92	0.92	0.92	0.91	0.90				
			Mean		1.02	1.02	1.04	1.04	1.05	1.06	1.05	1.04	1.09	1.06		
		1.5	L	2	1.01	1.03	1.03	1.02	1.03	1.05	1.04	1.06	1.06			
			L	1	0.85	0.87	0.88	0.88	0.91	0.95	0.98	1.01				
			W	2	1.02	1.00	1.00	1.00	1.00	1.00	1.00	1.00	1.00	1.00	1.00	1.00
			Mean		0.96	0.97	0.97	0.97	0.98	1.00	1.01	1.02	1.03	1.00	1.00	1.00
		1.25	P	1	1.03	1.02	1.04	1.04	1.04	1.04	1.04	1.06	1.09	1.03		
			P	0.5	0.92	0.95	1.01	1.04	1.08	1.09	1.07	1.07				
			W	2	1.00	1.00	1.00	1.00	1.00	1.00	1.00	1.00	1.00	1.00	1.00	1.00
			W	1	0.97	0.94	0.95	0.95	0.95	0.95	0.95	0.96				
			Mean		0.98	0.98	1.00	1.01	1.02	1.02	1.02	1.03	1.05	1.02	1.00	1.00
		Total mean			0.99	0.99	1.00	1.01	1.02	1.03	1.03	1.03	1.06	1.03	1.00	1.00
30	P, 2 kg	2.5	P	1	1.02	1.04	1.05	1.05	1.05	1.06	1.07	1.07	1.06	1.05		
			W	2	1.08	1.07	1.06	1.06	1.05	1.06	1.08	1.09	1.10	1.12		
			W	1	1.03	1.02	0.99	0.96	0.93	0.91	0.89	0.87				
			Mean		1.04	1.04	1.03	1.02	1.01	1.01	1.01	1.01	1.08	1.08		

		1.5	L	2	1.00	1.00	1.00	1.00	1.00	1.00	1.00	1.00	1.00	1.00	1.00	1.00
			L	1						0.93	0.93	0.97				
			W	2	1.00	1.00	1.00	1.00	1.00	1.00	1.00	1.00	1.00	1.00	1.00	1.00
			Mean		1.00	1.00	1.00	1.00	1.00	0.98	0.98	0.99	1.00	1.00	1.00	1.00
		1.25	P	1	0.98	0.96	0.91	0.88	0.85	0.82	0.81	0.77	0.80	0.81		
			P	0.5	1.02	1.04	1.04	1.02	1.00	0.97	0.95	0.91	0.92			
			W	2						0.85	0.83	0.84	0.99	0.94		
			Mean		1.00	1.00	0.98	0.95	0.93	0.88	0.86	0.84	0.90	0.88		
		Total mean			1.01	1.01	1.00	0.99	0.98	0.96	0.95	0.95	0.99	0.99	1.00	1.00
50	P, 2 kg	2.5	P	1	0.97	1.02	1.06	1.09	1.11	1.14	1.14	1.15	1.12	1.10		
			W	2	1.06	1.08	1.09	1.12	1.15	1.18	1.19	1.19	1.17			
			W	1	1.04	1.04	1.02	1.00	1.00	0.98	0.96	0.96				
			Mean		1.02	1.05	1.06	1.07	1.09	1.10	1.10	1.10	1.15	1.10		
		1.5	L	2	0.89	0.91	0.93	0.94	0.95	0.96	0.97	0.97	0.95			
			L	1	0.88	0.91	0.95	0.97	1.01	1.03	1.04	1.07				
			W	2	0.87	0.90	0.92	0.93	0.95	0.97	0.98	0.99	0.98			
			Mean		0.88	0.91	0.93	0.95	0.97	0.99	1.00	1.01	0 97			
		1.25	P	1	0.97	1.02	1.04	1.04	1.03	1.04	1.06	0.91	0.93	0.96		
			P	0.5	0.92	0.95	1.00	1.03	1.05	1.08	1.10	0.95				
			W	2	0.82	0.85	0.88	0.90	0.92	0.94	0.96	0.87	0.89			
			W	1	0.94	0.95	0.98	0.98	0.98	0.99	0.99	0.90				
			Mean		0.91	0.94	0.98	0.99	1.00	1.01	1.03	0.91	0.91	0.96		
		Total mean			0.97	0.98	0.99	1.00	1.00	1.00	1.00	0.96	0.99	0.99	1.00	1.00

of q can be considered to be almost straight and the $N-q_u$ curve in Fig. 37 was also nearly straight. Then the theoretical strain-m, q curves could be considered to be similar to empirical $N-\phi$ or $N-q_u$ curves.

The strains exerted at the end of the rod by impact are of course proportional to the total forces at the driving point of the penetration rod and it becomes difficult for a driving point to penetrate the soil layers in accordance with the increment of the total forces exerted at this point. As the resisting total forces at the driving point increase, the penetration index N increases in value. Thus the strain in Fig. 5 can be transformed to the penetration index N. q can also easily be transformed to the resisting strength of foundation soil, since q is proportional to the strength of the elastic k-bodies. Then it follows that the strain-m, q curves in Fig. 5 can be regarded as a theoretical basis of the empirical relations between the penetration index N, and the internal angle of friction ϕ of sandy soil or the unconfined compressive strength q_u of clayey soil, which were given by Terzaghi, Peck and others.

Summary

A theoretical treatment of dynamic penetration tests was given in Part I, as an application of the longitudinal vibration of a straight bar, and it has been proved that the fundamental equations and several predictions deduced from them were satisfactorily correct by the experiments in Part II. The theory and experiments included in this paper, however, were based on the assumption that a foundation soil behaves elastically, despite its inelasticity to a certain degree. Accordingly, the conclusions in each section can not always be applied to the practices of this sounding test, without any modification, but there are not a few case in the problems of soil mechanics, in which a solution of a problem concerning foundation soil, assuming it to be elastic, is applied to a practical object, for example Boussinesq's solution of stress propagation in semi-infinite elastic bodies. Therefore it may definitely be said that the conclusions in this paper may be a key to the solution of practical problems of dynamic penetration tests or pile driving.

The present author owes a great debt of gratitude to the Professors K. Manai, S. Kon, T. Sakai, C. Itakura and H. Yokomichi for their encouragements and advice throughout this investigation and also to Mr. S. Toki who has helped him in carrying out this investigation. He is indebted also to Miss E. Morishige and Miss Y. Kawahara and Mr. Mori for the stress calculations and the preparations of the manuscripts and to the Messers S. Iwama, M. Kimura and Y. Makabe in carrying out the experiments. He also expresses a deep sense of gratitude to Mr. L. Craighill who kindly corrected his English.

References

1) Love: Mathematical Theory of Elasticity, 431 (1934).
2) Timoshenko: Vibration Problems in Engineering, 397 (1937).
3) Timoshenko: Theory of Elasticity, 393 (1934).
4) Volterra, Barton: "An Impact Testing Machine for Plastics and Rubber-like Materials", Proc. Societ. Exper. Stress Analysis, XVI-1 157 (1959).
5) Granville and others: "An Investigation of the stress in reinforced concrete piles during driving", Building Research Technical Paper No. 20, London (1938).
6) Ohryoku-Sokutei-Gijitsu-Kenkyukai: Ohryoku-Sokuteihō, Tokyo, 186 (1955).
7) The letter to the present author from Oh-i K., one of the authors of the reference 6), a specialist in the field of stress measurement by strain gages in Japan, an Assistant Professor of Tokyo University.
8) Fukuoka Y.: Tsuchi to Kiso, Tokyo 4-2, 14 (1956).
9) Doshitsu Kōggakkai: Doshitsu-Shikenhō, Tokyo, 2nd Issue 254 (1959).
10) Gibbs, Holtz: "Research on Determining the Density of Sands by Spoon Penetration Test", Proc. 4th. Int. Conf. S. M. F. E. Vol. 1, 35 (1957).
11) In 404 page of the reference 2), it is said that, when m is less than 5, the maximum strain occurs in the first period and at the fixed end of the rod, but according to the solution by the present author, this limiting value of m was 5.6.